Christina B. Schroeter, Christopher Nelke, Marcus Schewe, Lucas Spohler, Alexander M. Herrmann, Thomas Müntefering, Niklas Huntemann, Maria Kuzikov, Philip Gribbon, Sarah Albrecht, Stefanie Bock, Petra Hundehege, Lea Christine Neelsen, Thomas Baukrowitz, Guiscard Seebohm, Bernhard Wünsch, Stefan Bittner, Tobias Ruck, Thomas Budde and Sven G. Meuth*

Validation of TREK1 ion channel activators as an immunomodulatory and neuroprotective strategy in neuroinflammation

https://doi.org/10.1515/hsz-2022-0266
Received August 30, 2022; accepted January 16, 2023;
published online February 14, 2023

Abstract: Modulation of two-pore domain potassium (K_{2P}) channels has emerged as a novel field of therapeutic strategies as they may regulate immune cell activation and metabolism, inflammatory signals, or barrier integrity. One of these ion channels is the TWIK-related potassium channel 1 (TREK1). In the current study, we report the identification and validation of new TREK1 activators. Firstly, we used a modified potassium ion channel assay to perform high-throughput-screening of new TREK1 activators. Dose-response studies helped to identify compounds with a high separation between effectiveness and toxicity. Inside-out patch-clamp measurements of *Xenopus laevis* oocytes expressing TREK1 were used for further validation of these activators regarding specificity and activity. These approaches yielded three substances, E1, B3 and A2 that robustly activate TREK1. Functionally, we demonstrated that these compounds reduce levels of adhesion molecules on primary human brain and muscle endothelial cells without affecting cell viability. Finally, we studied compound A2 via voltage-clamp recordings as this activator displayed the strongest effect on adhesion molecules. Interestingly, A2 lacked TREK1 activation in the tested neuronal cell type. Taken together, this study provides data on novel TREK1 activators that might be employed to pharmacologically modulate TREK1 activity.

Keywords: BL-1249; blood-brain barrier; electrophysiology; K_{2P} channels; TREK1; TRESK.

Christina B. Schroeter, Christopher Nelke, Marcus Schewe, Thomas Budde and Sven G. Meuth contributed equally to this work.

***Corresponding author: Sven G. Meuth**, Department of Neurology, Medical Faculty, Heinrich Heine University Düsseldorf, Moorenstr. 5, D-40225 Düsseldorf, Germany, E-mail: meuth@uni-duesseldorf.de
Christina B. Schroeter, Christopher Nelke, Alexander M. Herrmann, Thomas Müntefering, Niklas Huntemann, Stefanie Bock and Tobias Ruck, Department of Neurology, Medical Faculty, Heinrich Heine University Düsseldorf, Moorenstr. 5, D-40225 Düsseldorf, Germany
Marcus Schewe, Lea Christine Neelsen and Thomas Baukrowitz, Institute of Physiology, Christian-Albrechts University Kiel, Hermann-Rodewald-Straße 5, 24118 Kiel, Germany
Lucas Spohler, Sarah Albrecht and Petra Hundehege, Department of Neurology with Institute for Translational Neurology, University Hospital Münster, Albert-Schweitzer-Campus 1, D-48149 Münster, Germany
Maria Kuzikov and Philip Gribbon, Fraunhofer Institute for Translational Medicine and Pharmacology (ITMP), Schnackenburgallee 114, D-22525 Hamburg, Germany; and Fraunhofer Cluster of Excellence for Immune mediated diseases (CIMD), Theodor-Stern-Kai 7, D-60596 Frankfurt, Germany
Guiscard Seebohm, IfGH–Cellular Electrophysiology, Department of Cardiology and Angiology, University Hospital of Münster, Albert-Schweitzer-Campus 1, D-48149 Münster, Germany
Bernhard Wünsch, Institute for Pharmaceutical and Medicinal Chemistry, Westfälische Wilhelms-Universität Münster, Corrensstraße 48, D-48149 Münster, Germany
Stefan Bittner, Department of Neurology, University Medical Center Mainz, Langenbeckstraße 1, D-55131 Mainz, Germany
Thomas Budde, Institute of Physiology I, University of Münster, Robert-Koch-Straße 27A, D-48149 Münster, Germany

Introduction

Ion channels exhibit immunoregulatory properties. As such, they may regulate immune cell activation and metabolism, inflammatory signals or barrier integrity (Afzali et al. 2016; Bittner et al. 2014, 2013; Ruck et al. 2022). One of these ion channels is the mechanosensitive two-pore domain potassium (K^+) channel (K_{2P} channel) TWIK-related potassium channel 1 (TREK1). Belonging to the group of K_{2P} channels, TREK1 controls cell excitability by stabilizing the resting membrane potential (RMP) and modulating action potentials (APs) (Decher et al. 2021; MacKenzie et al. 2015). TREK1 channels respond to various stimuli. These include, among others, membrane stretch, intracellular pH, temperature, fatty acids or volatile anaesthetics (Decher et al. 2021). Expression of TREK1 has been mainly detected in the brain, but also in the heart, muscle, pancreas and prostate (Djillani et al. 2019). Thus, TREK1 has also been implicated in a

plethora of pathological conditions, including, but not limited to stroke, epilepsy, depression or inflammation (Djillani et al. 2019). In contrast to other K^+ channels like voltage-gated Kv channels or inwardly-rectifying Kir channels, K_{2P} channels, especially TREK1, function as a primarily selectivity filter (SF) gated ion channel (Lolicato et al. 2020; Schewe et al. 2016). This gate is sensitive to external K^+ concentrations, membrane voltage, the permanent ion species and pharmacological compounds (Lolicato et al. 2020, 2017; Schewe et al. 2019, 2016). Functionally, we previously described TREK1 as a regulator of blood-brain barrier (BBB) integrity (Bittner et al. 2014, 2013). In knockout mice lacking TREK1 ($TREK1^{-/-}$), cellular adhesion molecules were upregulated facilitating leukocyte trafficking into the central nervous system (CNS). Indeed, experimental autoimmune encephalomyelitis (EAE) was amplified in $TREK1^{-/-}$ mice accompanied by enhanced immune cell infiltration of the CNS (Bittner et al. 2013; Djillani et al. 2019, p. 1). Besides the upregulation of adhesion molecules, TREK1 also modifies endothelial cell (EC) microstructure further implicating TREK1 as regulator of immune cell trafficking across the BBB (Lauritzen et al. 2005). Immune cell infiltration is a pathogenic hallmark of neuroinflammation and BBB leakage has been reported in conditions such as multiple sclerosis (MS), stroke or neurodegenerative disorders (Bittner et al. 2014). Consequently, modulation of TREK1 has gained considerable interest as potential treatment target.

Broadly, we currently recognize two categories of TREK activators (Pope et al. 2018; Pope and Minor 2021; Schewe et al. 2019). First, activators such as BL-1249, fenamates, riluzole or C3001a affect all members of the TREK family including TREK1, TREK2 and TWIK-related arachidonic acid-stimulated K^+ (TRAAK) channel. The second group of compounds includes activators that act on TREK1 and TREK2 but not TRAAK. ML335, ML402, GI-530,159, and aristolochic acid are examples for such compounds. Currently, the negatively charged activator (NCA) BL-1249 still represents the most commonly employed TREK1 activator. However, BL-1249 lacks specificity potentially leading to activating effects also of non-target ion channels (Pope et al. 2018; Schewe et al. 2019). Mechanistically, structural studies of Lolicato et al. (2017) identified a group of small molecules (ML335 and ML402) activating TREK1 through direct SF stabilization (Lolicato et al. 2017). ML335 and ML402 utilize a 'cryptic' binding site behind the filter distinctly to the NCA binding site in the inner pore under the SF. Beyond that, several screening efforts over the last years identified further substances that are considered to be selective TREK channel activators like the dihydroacridine analogue ML67-33 for TREK1 (Bagriantsev et al. 2013) or 11-deoxy PGF2α, T2A3 (Dadi et al. 2017) and the CysLT1 antagonist pranlukast for TREK2 (Wright et al. 2019). Interestingly, the TREK1 activator ML67-33 that exhibits structural features of NCAs and additionally fits the NCA pharmacophore also activates other K_{2P} and Ca^{2+}-activated BK-type channels (Schewe et al. 2019). Therefore, the most substantial limitation of the currently available TREK1 activators is unspecific binding to and activation of other K^+ selective ion channels. To address this, we sought to identify new TREK1 channel activators and validate these substances for their modulatory potential *in vitro*. Harnessing new TREK1 activators could improve treatment strategies directed at ameliorating immune cell trafficking following inflammatory conditions.

Results

Assay validation

Here, we aimed to identify and characterize new TREK1 activators using a high-throughput-screening (HTS). To this end, we used the stably TREK1-transfected HEK293T (HEK293T/TREK1) cell line (Moha ou Maati et al. 2011). The TREK1-expressing vector was engineered with a geneticin resistance. The FluxOR™ Potassium Ion Channel Assay was adapted to detect TREK1 potassium ion channel activation in HEK293T cells (HEK293T) and HEK293T/TREK1 cells (Weaver et al. 2004) (Figure 1A). The assay principle is based on the ability of K_{2P} channels to pass thallium (Tl) ions as surrogates for potassium ions. Addition of Tl and/or channel activators results in opening of potassium channels by indirect (membrane depolarization) and direct (binding to the channel) effects, respectively. Cells are incubated with a non-fluorescent, Tl sensitive FluxOR dye. Once inside the cell, the dye is cleaved by intracellular esterases into a fluorogenic Tl sensitive dye, which remains in the cytosol. Upon Tl import, strong increase in fluorescence intensity can be observed due to binding of Tl to the FluxOR dye. To validate the FluxOR assay principle, we verified that there is no change to the fluorescence intensity without application of thallium in HEK293T/TREK1 cells (Figure 1B). Application of thallium elicited a fluorescence signal in dimethyl sulfoxide (DMSO)-treated HEK293T/TREK1 cells and non-transfected HEK293T cells. For investigation of potential TREK1 activators, HEK293T/TREK1 cells were seeded in 384-well plates and loaded with the FluxOR™ dye for 60 min. BL-1249 was selected as a well-established TREK1 activator to validate the assay (Tertyshnikova et al. 2005). HEK293T/TREK1 cells were incubated with increasing concentrations of BL-1249 for 20 min at room temperature (RT), followed by addition of Tl^+ and immediate readout of fluorescence signals (Figure 1C). Dose-dependent increase of fluorescence was observed with

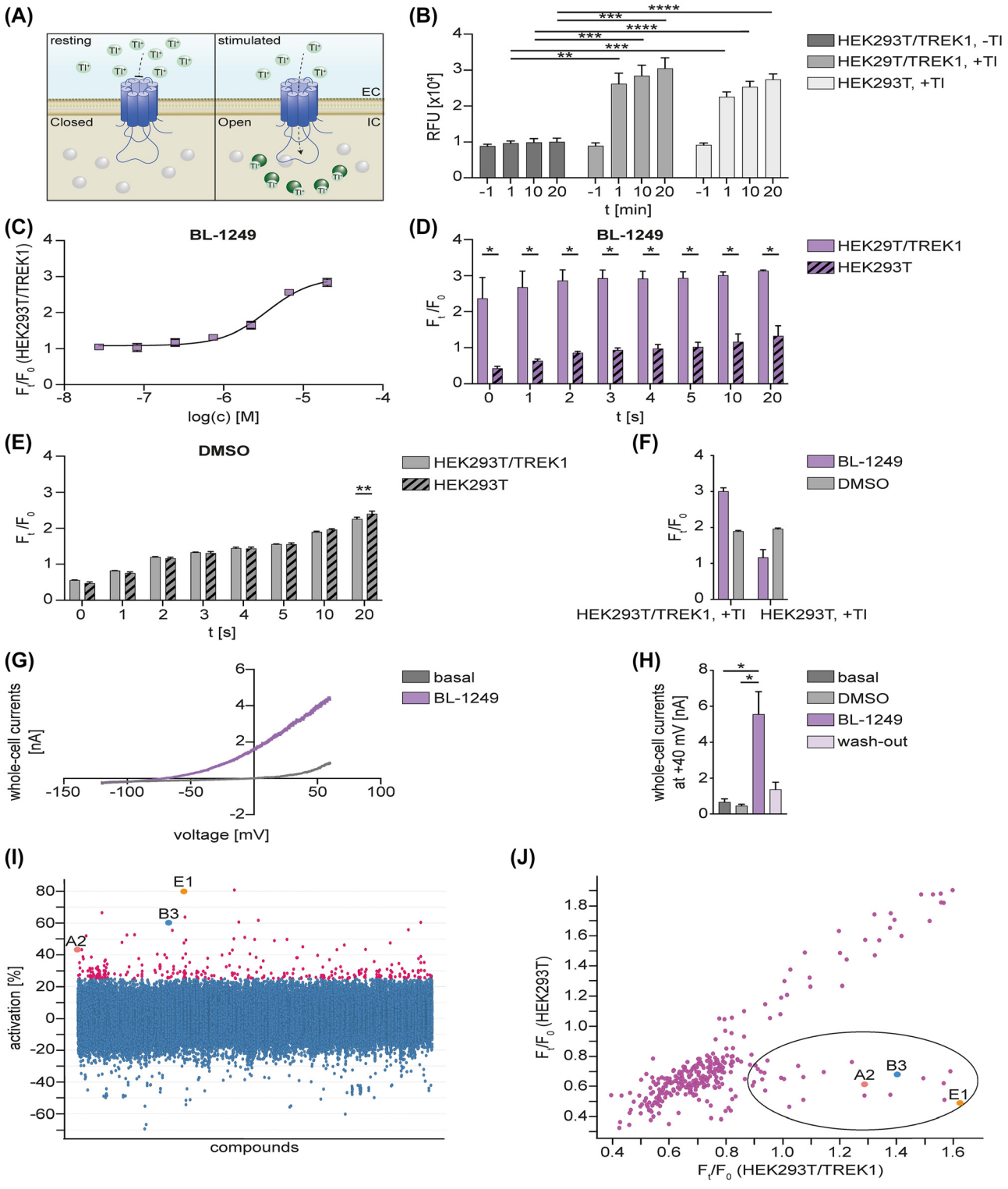

Figure 1: Adaptation of FluxOR™ potassium ion channel assay and its application for identification of new TREK1 channel activators. A: Schematic overview of assay principle. B: Increase in fluorescence in FluxOR™ dye loaded DMSO-treated HEK293T/TREK1 and HEK293T cells due to addition of Tl^+ as a surrogate for potassium (Two-way ANOVA with Tukey's multiple comparisons test, $n = 4$ for all groups). C: HEK293T/TREK1 cells were incubated with increasing concentrations of BL-1249 (logarithmic concentrations are depicted in [M]) for 20 min at RT, followed by fluorescence detection using FluxOR™ potassium ion channel assay. $EC_{50} = 3.51$ µM ($n = 2$). D: FluxOR™ dye loaded cells were incubated with BL-1249 for 20 min at RT before addition of Tl^+. Enhancement of fluorescence response in HEK293T/TREK1 cells due to activation of TREK1 using 200 µM of BL-1249. No enhancement of fluorescence response in HEK293T cells (Two-way ANOVA with Šidák's multiple comparisons test, $n = 3$ for both groups). E: Increase in fluorescence in FluxOR™ dye

calculated EC_{50} of 3.51 µM, confirming previously reported values (Tertyshnikova et al. 2005). Concentrations of BL-1249 were tested on HEK293T/TREK1 and non-transfected HEK293T cells. To validate the FluxOR assay, we applied 200 µM of BL-1249 as positive control (Figure 1D) and 1% DMSO as negative control (Figure 1E). DMSO did only affect fluorescence intensity for t = 20 s, while BL-1249 resulted in a significant increase of the fluorescence signal at all time points (0–20 s). No enhancement of fluorescence response was observed in non-transfected HEK293T cells compared to DMSO control, confirming specificity of TREK1 activation by BL-1249 (Figure 1F).

To verify TREK1 activation by BL-1249, we performed whole-cell measurements of HEK293T/TREK1 cells under basal (control) conditions, in the presence of BL-1249, after wash-out of BL-1249 and in the presence of the solvent DMSO, respectively (Figure 1G, H). Here, treatment with BL-1249 increased TREK1 currents significantly compared to DMSO alone.

Marker library generation and HTS of potential TREK1 activators

In order to confirm assay suitability for HTS, a marker library was screened. ENZO SCREEN-WELL® FDA approved drug library V2 containing 774 compounds was selected to identify TREK1 activators among approved drugs. Compounds were tested at 25 µM after 20 min incubation at RT in cell cultures. Each assay plate included BL-1249 at 125 µM and DMSO 0.5 v/v % as controls, representing 100% activation and 0% activation, respectively. All plates showed a Z' > 0.5, confirming suitability for HTS (Table 1). The Z' factor determines the assay reliability, with high reliability expected at values between 0.5 and 1.0. Among tested library compounds hexachlorophene showed strongest activation (64.18%) of HEK293T/TREK1 cells (Table 2). Hexachlorophene is a known potent activator of the potassium voltage-gated channel subfamily Q member 1 (KCNQ1) ion channel which is endogenously expressed in HEK293T cells (Zheng et al. 2012). Therefore, the results showed the general suitability of the assay to identify compounds functionally interacting with potassium channels. Enamine collection (https://enamine.net) was used to identify new small molecule activators of TREK1. For the final HTS-experiment, 104 192 compounds were selected from the Enamine® substance library and screened at single concentrations of 10 µM using previously optimized conditions. All assay plates were controlled to pass the criteria for HTS with a Z' > 0.5. Compounds showing ≥ 25% activation of TREK1 compared to controls (BL-1249 representing 100% activation and DMSO representing 0% activation) were defined as hits, resulting in 303 hit-compounds (0.29% hit rate) (Figure 1I).

These 303 hits were confirmed for their activity in HEK293T/TREK1 cells and in non-transfected HEK293T cells using their screening concentrations of 10 µM (in triplicates). 26 compounds were identified as selective for activation of TREK1 (Figure 1J) and were further characterized in dose-response studies. In order to assess the activity towards TREK1, compounds were incubated for 20 min at RT. In this period, no toxic effects were observed. In order to assess putative cytotoxicity of identified hits, we incubated cells for

Table 1: Calculated Z′ values of the marker library screen.

Compound plate	Z'
ENZ_0000005_L03	0.56
ENZ_0000004_L03	0.51
ENZ_0000003_L03	0.55

Z' calculation was used for assessment of quality of screened plates. All assay plates were controlled to pass the criteria for HTS with a Z' > 0.5. HTS, high-throughput-screening.

loaded HEK293T/TREK1 and HEK293T cells after addition of 1% DMSO representing unspecific Tl^+ transport (Two-way ANOVA with Šidák's multiple comparisons test, n = 3 for both groups). F: HEK293T/TREK1 and HEK293T cells were incubated with 200 µM BL-1249 or 1% DMSO for 20 min at RT, followed by fluorescence detection using FluxOR™ potassium ion channel assay (Two-way ANOVA with Tukey's multiple comparisons test, n = 3 for both groups, p > 0.05). G: Representative traces of wt TREK1 K_{2P} channel currents from whole-cell experiments using HEK293T cells. Voltage ramps were measured between −100 mV and +60 mV and analysed at +40 mV. Measurements were performed in control solution ('basal', pH 7.3) and in the presence of 125 µM BL-1249. H: Summary plot showing TREK1 K_{2P} channel currents from measurements as in G, at basal conditions (n = 6), in the presence of 0.25% DMSO (n = 3), in the presence of 125 µM BL-1249 (n = 6; FI = 9.29 ± 2.01) and after wash-out of BL-1249 (n = 4). TREK1 currents were significantly increased by BL-1249 (Kruskal–Wallis test including Dunn´s post-hoc test, p = 0.0135 for basal vs. BL-1249, p = 0.0133 for DMSO vs. BL-1249, p > 0.05 for remaining data). I: Calculated TREK1 activation in % of screened compounds normalized to TREK1 activation by BL-1249 (100% activation) and DMSO (0% activation). Substances with TREK1 activation of ≥25% are coloured in magenta. J: Hit confirmation of selected hits in HEK293T/TREK1 and HEK293T cells, tested at 10 µM in triplicates. Data show average values of signal increase ratios. Compounds with observed activation in HEK293T/TREK1 cells and no activation in HEK293T cells are encircled in black. Abbreviations: DMSO, dimethyl sulfoxide; EC, extracellular; EC_{50}, half maximal effective concentration; F_0, minimal fluorescence (arbitrary units); F_t, steady-state terminal fluorescence (arbitrary units); F_t/F_0, signal increase ratio; HEK293T, HEK293T cells; HEK293T/TREK1, stably TREK1-transfected HEK293T cells; IC, intracellular; min, minutes; K_{2P} channel, two-pore domain potassium channel; mV, millivolt; nA, nanoampere; RFU, relative fluorescence unit; RT, room temperature; s, seconds; SEM, standard error of the mean; t, time; Tl, thallium; TREK1, TWIK-related potassium channel 1; wt, wild type.

Table 2: Potassium ion channel activators identified in the marker library screen.

Name	TREK1 activation [%]
Nisoldipine	21.16
Bexarotene	47.82
Hexachlorophene	**64.18**
Ciclopirox	30.85
Aprepitant	44.95
Mitotane	25.28
Permethrin	23.66

TREK1 activation in % is indicated for tested library compounds. Hexachlorophene showed strongest activation (64.18%) of HEK293T/TREK1 cells. HEK293T/TREK1, stably TREK1-transfected HEK293T cells; TREK1, TWIK-related potassium channel 1.

48 h. The effect on cell viability was observed using the Promega CellTiter-Glo assay which is based on detection of intracellular adenosine triphosphate (ATP) in metabolically active cells. Based on these results, we selected 17 substances with a half maximal effective concentration (EC_{50}) smaller than the 50% cytotoxic concentration (CC_{50}). Z220539848 ('E1'), Z27879940 ('B3') and Z56776203 ('A2') showed best separation between cytotoxicity and TREK1 activation (Supplementary Figure 1). Structural formulas of these three compounds are shown in Supplementary Figure 1.

Hit validation

Next, we further investigated the 17 substances identified in the previous section for their ability of TREK1 activation. For this purpose, we performed inside-out patch-clamp measurements of TREK1 expressing *Xenopus* oocytes to determine the individual dose-response curves for all 17 substances. We tested the TREK1 activation by the selected compounds as well as their influence on currents through TWIK-related spinal cord potassium channel (TRESK) channels (exemplary measurement of TREK1 activation under increasing concentrations of compound E1 is displayed in Figure 2A). Based on these experiments and previous FluxOR and CellTiter Glo assay results (Figure 1, Supplementary Figure 1), we selected 11 substances for further testing (Table 3).

Next, we chose the three most promising of these compounds based on the following criteria: (1) their TREK1 activation rate (i.e. fold increase (FI) at −80 mV), (2) a high separation between activation (EC_{50}) and cytotoxicity (CC_{50}) and (3) their interaction with other K_{2P} channels (Table 3). The latter was assessed for TRESK (measured by the half maximal inhibitory concentration (IC_{50}), referring to the substance concentration for 50% blockage of TRESK). Eventually Z220539848 ('E1') (Figure 2B), Z27879940 ('B3') (Figure 2C) and Z56776203 ('A2') (Figure 2D) were chosen. Interestingly, these substances displayed high TREK1 activation while also inhibiting the related K_{2P} channel TRESK (Figure 2B–D). Strikingly, the inhibitory effect on TRESK was stronger than the activating effect on TREK1 for E1 and B3 (IC_{50} – TRESK was lower than EC_{50} – TREK1), but not for A2 (8.56 ± 1.05 µM (EC_{50} – TREK1) versus 11.59 ± 1.75 µM (IC_{50} – TRESK)) (Table 3). For each of these three compounds, the respective EC_{50} dose was used for all further experiments. Finally, we measured the effect of 10 µM A2 (~EC_{50} concentration for TREK1) for all K_{2P} channels that can be expressed in the plasma membrane. Interestingly, A2 only showed an activating effect of the closest TREK1 (FI at −80 mV = 57 ± 11 µM, n = 27) homologue TREK2 (FI at −80 mV = 31 ± 11 µM, n = 15), a weak inhibitory effect of the distantly related K_{2P}s TASK-3 and TRESK and almost no effect on all others (Figure 2E).

Functional validation of compounds in the inflammatory setting

In a next step, we aimed to investigate the functional properties of E1, B3 and A2. Therefore, we performed a functional stimulation assay in primary human muscle cells (PHMCs) and primary human microvascular endothelial cells (PHMECs) (Figure 3A). Cells were cultivated for 24 h (t = 0–24 h) before further processing. Then, cells were stimulated with 500 U/mL tumour necrosis factor alpha (TNF-α) for 24 h (t = 24–48 h). Thereafter, cells were then washed and cultivated in normal medium for another 24 h ("wash-out", t = 48–72 h) since TREK1 expression levels are downregulated upon stimulation. At each particular time, the mean fluorescence intensity (MFI) was recorded by flow cytometry for major histocompatibility complex 1 (MHC-I), major histocompatibility complex 2 (MHC-II) and intercellular adhesion molecule 1 (ICAM-1) on PHMCs. For PHMECs, we analyzed vascular cell adhesion molecule 1 (VCAM-1) instead of MHC-II. Values were normalized to BL-1249 treated cells. Functionally, in PHMCs, A2 decreased MHC-I levels before and after stimulation as well as ICAM-1 levels during and after stimulation as compared to BL-1249 (n = 3) in PHMCs (Figure 3B). B3 and E1 treatment led to increased MHC-I levels during stimulation. In PHMECs, A2 decreased MHC-I levels during and after stimulation with TNF-α as compared to BL-1249 (n = 3) (Figure 3C). ICAM-1 and VCAM-1 levels were also decreased in response to A2 treatment after stimulation. In comparison with BL-1249, B3 treatment resulted in enhanced ICAM-1 and VCAM-1 levels after stimulation. E1 decreased MHC-1 during and after stimulation, while

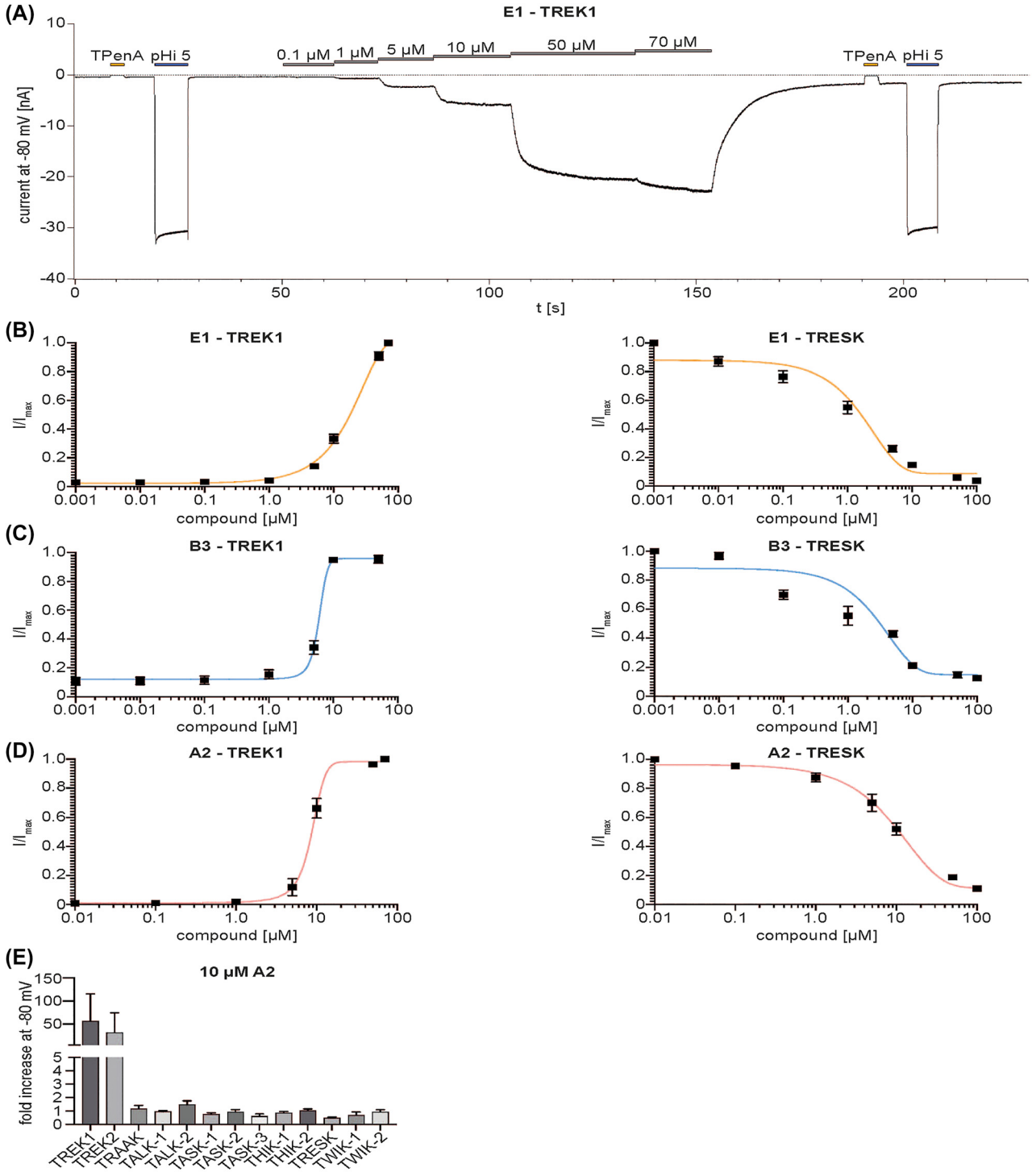

Figure 2: Electrophysiological compound validation of TREK1 activating compounds. A: Representative measurement of wt TREK1 K_{2P} channels from inside-out patches of *Xenopus laevis* oocytes showing the activation by increasing concentrations of the indicated compound E1, recorded at a constant potential of −80 mV in symmetrical K^+ at pH 7.4. Patch integrity was tested by application of 1 mM TPenA showing almost full block of TREK1 baseline current. Channel opening by intracellular acidification (pH_i 5.0) was measured as reference activation. B–D: Dose-response curves from measurements as in A for TREK1 (left panels) and TRESK K_{2P} channels (right panels) showing the concentration-dependent activation of TREK1 and inhibition of TRESK (mean ± SEM) respectively, with the compounds E1 (B), B3 (C) and A2 (D) Compounds were chosen due to the ratio of (i) fold current increase (FI), (ii) the difference between EC_{50} and CC_{50}, (iii) as well as their interaction with TRESK K_{2P} channels (IC_{50}). E: Modulation of K_{2P} channel currents by 10 µM A2, analysed at −80 mV (One-way ANOVA p-values: TREK1 vs. TREK2 0.0202, TREK1 vs. TRAAK 0.0004, TREK1 vs. TALK-1 0.0002, TREK1 vs. TALK-2 <0.0001, TREK1 vs. TASK-1 0.0003, TREK1 vs. TASK-2 0.0004, TREK1 vs. TASK-3 0.0003, TREK1 vs. THIK-1 0.0002, TREK1 vs. THIK-2 0.0002, TREK1 vs. TRESK <0.0001, TREK1 vs. TWIK-1 0.0003, TREK1 vs. TWIK-2 0.0004). Abbreviations: CC_{50}, 50% cytotoxic concentration; EC_{50}, half maximal effective concentration; FI, fold increase; I, current; IC_{50}, half maximal inhibitory concentration; I_{max}, maximum current; K_{2P} channel, two-pore domain potassium channel; mV, millivolt; nA, nanoampere; pH_i, intracellular pH; s, seconds; SEM, standard error of the mean; *t*, time; TPenA, Tetra-pentyl-ammonium; TREK1, TWIK-related potassium channel 1; TRESK, TWIK-related spinal cord potassium channel; wt, wild type.

Table 3: Properties of 11 selected experimental TREK1 activators.

Cmp	Name	ID	EC_{50} -TREK1 (patch) [µM]	FI (−80 mV) -TREK1	EC_{50} -TREK1 (FluxOR), 95% confidence interval [µM]	CC_{50} (CellTiter-Glo), 95% confidence interval [µM]	IC_{50} -TRESK (patch) [µM]	Max. inhib. -TRESK (patch) [%]
Cmp 1	F1	Z133668732	9.45 ± 1.24 (*n* = 15)	18.36 ± 3.80 (*n* = 15)	3.93, 2.73–5.65 (*n* = 3)	72.44, 0.13–42,070 (*n* = 3)	0.97 ± 0.17 (*n* = 10)	83.40 ± 1.46 (*n* = 10)
Cmp 2	E1	Z220539848	16.84 ± 1.30 (*n* = 11)	50.14 ± 10.50 (*n* = 11)	7.08, 6.06–8.28 (*n* = 3)	46.77, 28.99–74.1 (*n* = 3)	1.56 ± 0.28 (*n* = 10)	96.24 ± 0.49 (*n* = 10)
Cmp 3	B3	Z27879940	5.86 ± 0.19 (*n* = 12)	19.58 ± 5.02 (*n* = 12)	4.61, 3.29–6.46 (*n* = 3)	134.89, 0.33–54,900 (*n* = 3)	1.09 ± 0.45 (*n* = 9)	85.15 ± 1.92 (*n* = 9)
Cmp 4	B5	Z29191102	7.03 ± 0.28 (*n* = 11)	41.54 ± 10.75 (*n* = 11)	7.63, 6.01–9.68 (*n* = 3)	30.9, 9.36–101.4 (*n* = 3)	0.31 ± 0.12 (*n* = 8)	91.38 ± 1.85 (*n* = 8)
Cmp 5	F2	Z46391446	9.21 ± 1.15 (*n* = 14)	15.49 ± 3.47 (*n* = 14)	3.34, 2.15–5.19 (*n* = 3)	23.44, 19.54–28.33 (*n* = 3)	1.50 ± 0.21 (*n* = 9)	94.80 ± 0.62 (*n* = 9)
Cmp 6	F3	Z30791069	N. A. (*n* = 11)	128.21 ± 33.19 (*n* = 11)	21.4, 16.27–28.15 (*n* = 3)	66.07, 2.87–1517 (*n* = 3)	2.02 ± 0.20 (*n* = 9)	59.32 ± 1.62 (*n* = 9)
Cmp 7	C4	Z247322124	15.93 ± 4.45 (*n* = 11)	5.07 ± 0.81 (*n* = 11)	9.18, 5.51–15.28 (*n* = 3)	67.61, 1.35–3359 (*n* = 3)	2.39 ± 0.36 (*n* = 7)	96.76 ± 0.45 (*n* = 7)
Cmp 8	A2	Z56776203	8.56 ± 1.05 (*n* = 10)	156.78 ± 32.49 (*n* = 10)	6.29, 4.68–8.46 (*n* = 3)	44.67, 31.87–61.76 (*n* = 3)	11.59 ± 1.75 (*n* = 4)	92.50 ± 0.46 (*n* = 4)
Cmp 9	A4	Z73346473	N. A. (*n* = 10)	18.49 ± 3.08 (*n* = 10)	18.51, 13.01–26.34 (*n* = 3)	147.91, 0.06–326,400 (*n* = 3)	79.16 ± 14.09 (*n* = 8)	63.41 ± 2.89 (*n* = 8)
Cmp 10	B4	Z90696735	N. A. (*n* = 11)	147.91 ± 31.92 (*n* = 11)	13.19, 8.02–21.68 (*n* = 3)	57.54, 1.86–1789 (*n* = 3)	1.38 ± 0.21 (*n* = 8)	94.53 ± 0.64 (*n* = 8)
Cmp 11	B2	Z70910938			15.70, 11.83–20.84 (*n* = 3)	72.44, 13.32–388.8 (*n* = 3)		

Detailed characteristics of TREK1 activating compounds tested via FluxOR ('FluxOR') and CellTiter-Glo ('CellTiter-Glo') assay in HEK293T/TREK1 cells followed by inside-out macropatch-clamp recordings of *X. laevis* oocytes ('patch'). Concentrations (mean ± SEM) are indicated in µM. Compound 11 was not tested in patch-clamp experiments, hence values for EC_{50} – TREK1 (patch) and IC_{50} – TRESK (patch) are missing. The three final substances (E1, orange; B3, blue; A2, red) were chosen due to their activation rate (FI), a clear separation between EC_{50} and CC_{50} and their interaction potential with other K_{2P} channels, such as TRESK (IC_{50}). CC_{50}, 50% cytotoxic concentration; Cmp, compound; EC_{50}, half maximal effective concentration; FI, fold increase; HEK293T/TREK1, stably TREK1-transfected HEK293T cells; IC_{50}, half maximal inhibitory concentration; max. inhib., maximal inhibition; N.A., not applicable; TREK1, TWIK-related potassium channel 1; TRESK, TWIK-related spinal cord potassium channel.

VCAM-1 increased before and during stimulation. All changes were interpreted as changes compared to BL-1249. Next, we investigated the functional effects of E1, B3 and A2 by assessing cell adhesion and transmigration. We employed a functional low physiological flow (0.25 dyn/cm^2) assay to characterize adhesion and a Boyden chamber assay to assess transmigration of immune cells on/through a confluent EC monolayer (*n* = 3) (Figure 3D). First, stimulated peripheral blood mononuclear cells (PBMCs) were applied for 30 min under low flow (0.25 dyn/cm^2) after washout of TNF-α (*t* = 72 h). As EC barrier, we employed PHMECs. PHMECs were treated with either 1% DMSO, BL-1249, E1, B3 or A2. Adherent immune cells were counted per 20 x high-power field (HPF). Here, we observed no differences between the three different compounds at *t* = 72 h (*n* = 3) (Figure 3E). We also determined the number of transmigrated cells through the EC layer (*n* = 3) (Figure 3F). E1, B3 and A2 as well as the control compound BL-1249 revealed no statistical differences. Next, we studied the proliferation rate of ECs in response to our experimental compounds. Therefore, we quantified the

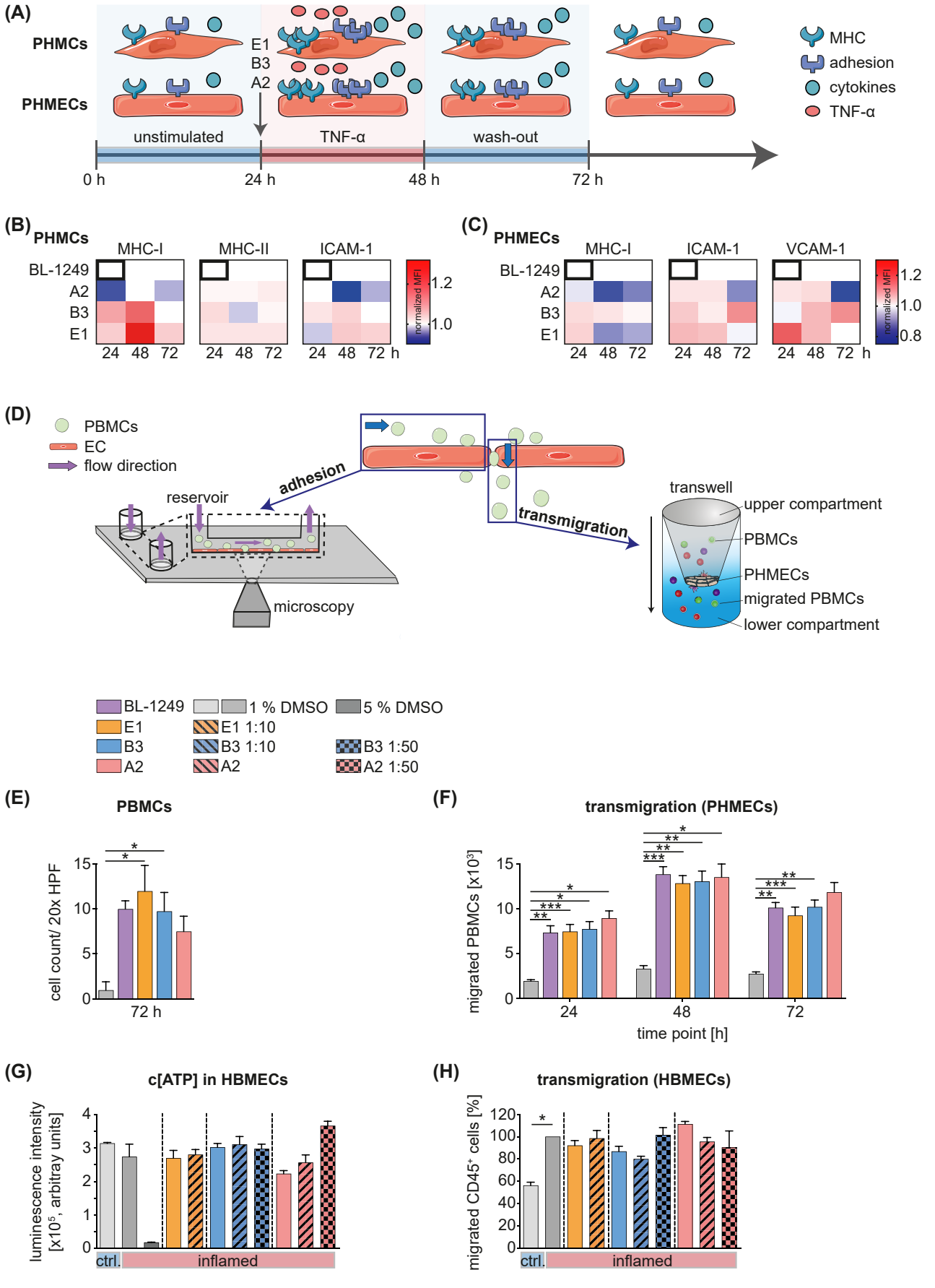

Figure 3: Functional validation of experimental TREK1 activators. A: Schematic overview of functional assays. PHMCs or PHMECs were incubated for 24 h (0–24 h). Afterwards, cells were stimulated with TNF-α for 24 h (24–48 h). Cells were washed after stimulation (48–72 h). B/C: MFIs were quantified by flow

metabolic state of human brain microvascular endothelial cells (HBMECs) by assessment of ATP concentrations. To mimic cellular inflammation, HBMECs were inflamed with 100 U/mL of interferon-gamma (IFN-γ) and TNF-α while applying E1, B3 or A2. Naïve (i.e. not inflamed) and DMSO-treated cells were used as controls. Compounds were applied in doses of their respective EC_{50} and dilution rates of 1:10 and 1:50 of their EC_{50}. HBMEC survival was higher for A2 at a dilution of 1:50, although without reaching statistical significance (n = 3) (Figure 3G), whereas the other compounds displayed no significant changes. Finally, we assessed the migration of $CD45^+$ leukocytes over inflamed HBMECs in a transwell insert for each compound at the same dilution rates of EC_{50} as in Figure 3G. Treatment with 100 U/mL of IFN-γ and TNF-α was used for stimulation. DMSO was employed as control. Here, no statistically significant influence on leukocyte migration levels was observed for any of the compounds.

Whole-cell voltage-clamp recordings: impact of BL-1249 and spadin on the I_{SO} in neurons of the ventrobasal thalamic complex

Since A2 displayed the smallest interaction potential with TRESK (Figure 2, Table 3) and the strongest effect on levels of adhesion molecules (Figure 3), we aimed to better understand its potential effects in a biological system. From a translational perspective, application of a TREK1 activator could also affect cellular homeostasis beyond the BBB. Independent of validating the influence of A2 on TREK1, we sought to study its effect on the TREK1 current expressed by thalamocortical relay (TC) neurons. These neurons are well known to express functional TREK1 channels (Bista et al. 2012, 2015b) and BK channels (Ehling et al. 2013). In consequence, these cells represent interesting targets to assess the summed main (on TREK channels) and side (on other ion channels) effects of TREK modulators that may pass the BBB. Therefore, we first tested BL-1249 in voltage-clamp experiments in TC neurons of the ventrobasal thalamic complex (VB) in wild type (wt) C57BL/6J and $TREK1^{-/-}$ mice at a concentration of 10 µM to prove that the experimental setup was suitable to display TREK1 currents and to acquire reference values for validation of A2.

To investigate, whether the substances have an impact on the TREK1 current, we applied a typical ramp protocol suited to study of K_{2P} channels (Meuth et al. 2003; Millar et al. 2000). The percentage change of the standing outward current (I_{SO}) was analyzed at −20 mV (Figure 4A). To assess the specificity of the substances, experiments were performed in wt C57BL/6J and $TREK1^{-/-}$ mice. Mean sensitive currents were analyzed.

In both, wt and $TREK1^{-/-}$ C57BL/6J mice, BL-1249 increased the I_{SO} by a comparable amount (11.6 ± 2.4% in wt C57BL/6J mice vs. 11.7 ± 4.4% in $TREK1^{-/-}$, p > 0.05, Figure 4B). Figure 4C shows an exemplary recording of a VB neuron in wt C57BL/6J mice before and after the application of 10 µM BL-1249. The increase of the I_{SO} is depicted. The mean sensitive current of the recordings with BL-1249 in wt C57BL/6J mice (Figure 4D), obtained by subtracting the currents before and after the substance was washed in, indicated a reversal potential at −75 mV and a distinct outward rectifying component.

Spadin is a specific blocker of TREK1 (Mazella et al. 2010). For voltage-clamp experiments, spadin at concentrations of 1 µM and 10 µM was tested in VB neurons of wt

cytometry of PHMCs and PHMECs. MFIs were normalized to BL-1249 treated cells. MFIs were measured at three time points (24 h, 48 h and 72 h; n = 3 for each group). D: Schematic principle of the functional low physiological flow assay (left): PBMCs were passed through a reservoir lined with a confluent EC monolayer of PHMECs. Adherent cells were quantified by microscopy. Schematic principle of transmigration assay (right): A transwell insert was lined with confluent PHMECs. PBMCs were added and counted upon reaching the lower compartment. E: Quantification of the functional low physiological flow assay. Stimulated PBMCs were applied for 30 min under a flow of 0.25 dyn/cm^2 after washout of TNF-α (t = 72 h). PHMECs were used as EC layer and treated with either 1% DMSO, BL-1249, A2, B3 or E1. PBMCs were counted per 20x HPF (Kruskal–Wallis test with Dunn's post-hoc test, n = 4 for all groups, p > 0.05 for three test compounds and control compound BL-1249). F: Quantification of the transmigration assay. PBMCs were added to a PHMEC monolayer treated with either 1% DMSO, BL-1249, A2, B3 or E1. Transmigrated PBMCs were counted by flow cytometry (Kruskal–Wallis test with Dunn's post-hoc test, n = 6–8 for all groups, p > 0.05 for three test compounds and control compound BL-1249). G: Proliferation of HBMECs measured by luminescence intensity of ATP. HBMECs were treated with 100 U/mL of TNF-α and INF-γ ('inflamed') followed by application of either A2, B3 or E1, respectively (Kruskal–Wallis test with Dunn's post-hoc test, n = 3 for all groups, p > 0.05). H: Quantification of $CD45^+$ leukocytes that migrated through an HBMEC monolayer. HBMECs were treated with DMSO and 100 U/mL of TNF-α and IFN-γ ('inflamed') or DMSO alone ('ctrl'). HBMECs were also treated with the indicated compounds and dilution series (Kruskal–Wallis test with Dunn's post-hoc test, n = 3 for all groups, p > 0.05). Abbreviations: ATP, adenosine triphosphate; ctrl, control; DMSO, dimethyl sulfoxide; EC, endothelial cell; h, hour/s; HPF, high-power field; HBMECs, human brain microvascular endothelial cells; ICAM-1, intercellular adhesion molecule 1; IFN-γ, interferon-gamma; MHC-I, major histocompatibility complex 1; MHC-II, major histocompatibility complex 2; PBMCs, peripheral blood mononuclear cells; PHMECs, primary human microvascular endothelial cells; PHMCs, primary human muscle cells; SEM, standard error of the mean; TNF-α, tumour necrosis factor alpha; VCAM-1, vascular cell adhesion protein 1.

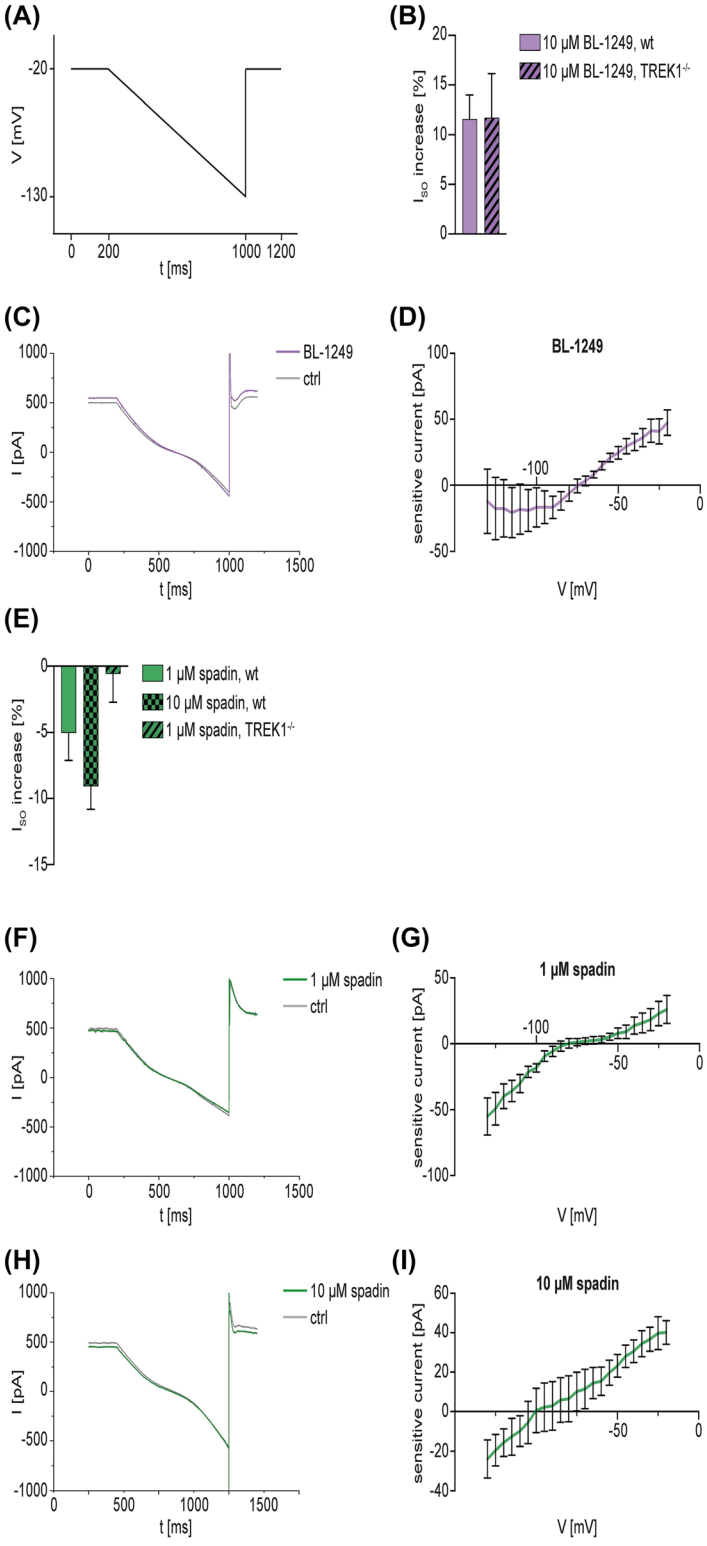

Figure 4: Whole-cell voltage-clamp recordings in VB neurons of wt C57BL/6J and TREK1$^{-/-}$ mice after treatment with the TREK1 activator BL-1249 or the TREK1 blocker spadin. A: Ramp protocol used for voltage-clamp experiments. Cells were first held at −20 mV for 200 ms, then hyperpolarized to −130 mV over 800 ms, followed by another step at −20 mV for 200 ms. The I_{SO} was measured before and after the substance was washed into the external bath solution and its increase [%] was calculated. Sensitive currents were calculated by graphically subtracting the currents before and after the substance was washed in. B: Effects of BL-1249 on the I_{SO} in VB neurons of wt C57BL/6J and TREK1$^{-/-}$ mice. 10 µM of BL-1249 were applied (unpaired Mann-Whitney *U* test, $n = 6$ wt, $n = 5$ – TREK$^{-/-}$, $p > 0.05$). C: Exemplary recording of a VB neuron in wt C57BL/6J mice before (grey trace) and after (violet trace) the application of 10 µM BL-1249. D: Mean sensitive currents of voltage-clamp recordings in VB neurons of wt C57BL/6 mice after treatment with 10 µM BL-1249 (reversal potential at −75 mV). E: Effect of spadin on the I_{SO} in VB neurons of wt C57BL/6J and TREK1$^{-/-}$ mice. Concentrations of both 1 µM (in wt C57BL/6J and TREK1$^{-/-}$ mice) and 10 µM (in wt C57BL/6J mice) spadin were tested. Increases of I_{SO} [%] are depicted (Kruskal–Wallis test with Dunn´s post-hoc test, $n = 5$ for all groups, $p > 0.05$). F, H: Exemplary recording of VB neurons in wt C57BL/6J mice before (grey trace) and after (green trace) the application of spadin (1 µM, F; 10 µM, H). G, I: Mean sensitive currents of voltage-clamp recordings in VB neurons of wt C57BL/6 mice after treatment with 1 µM (G, equilibrium potential at −80 mV) or 10 µM spadin (I, equilibrium potential at −100 mV), respectively. Abbreviations: Ctrl, control; DMSO, dimethyl sulfoxide; I, current; I_{SO}, standing outward current; ms, milliseconds; mV, millivolt; pA, picoampere; s, seconds; SEM, standard error of the mean; *t*, time; TREK1, TWIK-related potassium channel 1; TREK1$^{-/-}$, TREK1 knockout; V, voltage; VB, ventrobasal thalamic complex; wt, wild type.

C57BL/6J mice. 1 µM spadin was additionally tested in TREK1$^{-/-}$ mice. In wt C57BL/6J mice, spadin showed a dose-dependent decrease of the I_{SO} with 1 µM reducing the I_{SO} by 5.0 ± 2.1% and 10 µM by 9.1 ± 1.7%, respectively. When tested in TREK1$^{-/-}$ mice at a concentration of 1 µM, spadin only reduced the I_{SO} by 0.6 ± 2.1% ($p > 0.05$ for all results, Figure 4E). Exemplary traces of recordings with 1 µM (Figure 4F) and 10 µM (Figure 4H) spadin illustrated the

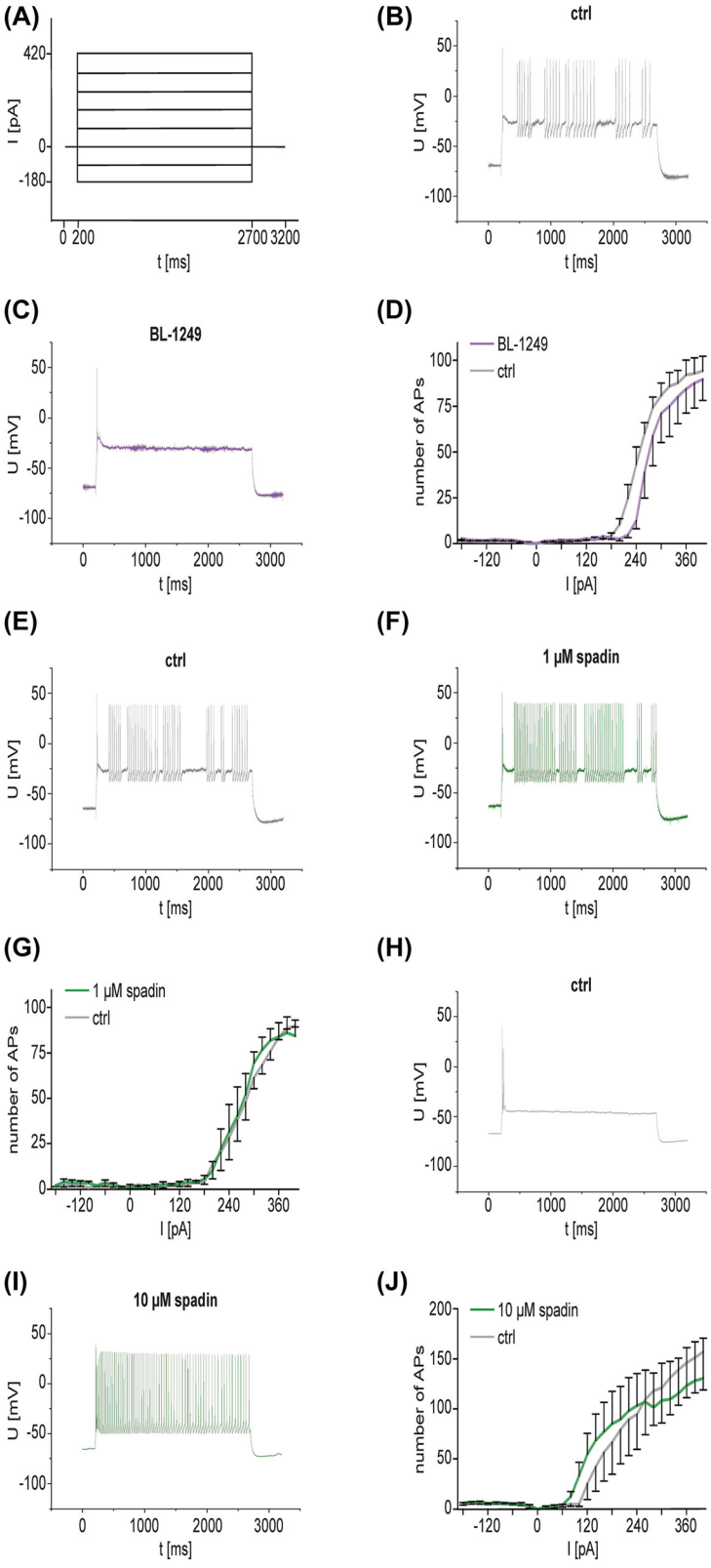

Figure 5: Whole-cell current-clamp experiments in murine VB neurons in wt C57BL/6J mice after treatment with TREK1 activator BL-1249 or the TREK1 blocker spadin. A: Step protocol used for current-clamp experiments. All experiments were performed at RMP (ranging from −60 to −70 mV). From the RMP, a current step protocol was applied with each step of the protocol increasing the current injected by +20 pA and lasting for 2500 ms. Injected currents ranged from −180 pA to +420 pA. B, C: Exemplary recording of a VB neuron before (B) and after the treatment with 10 µM BL-1249 (C). In both cases, a depolarizing current step of 260 pA was applied. D: Input-output curve of VB neurons in wt C57BL/6J mice before (grey trace) and after (violet trace) treatment with 10 µM BL-1249. The curve was generated by plotting the number of APs generated against the injected current (Mixed-effects analysis with Šidák correction, F (1, 8) = 0.6765, n = 5 for both groups, $p > 0.05$). E, F: Exemplary recording of a VB neuron before (E) and after (F) the treatment with 1 µM spadin. In both cases, a depolarizing current step of +320 pA was applied. G: Input-output curve of VB neurons in wt C57BL/6J mice before (grey trace) and after (green trace) application of 1 µM spadin (Mixed-effects analysis with Šidák correction, F (1, 6) = 0.07941, n = 4, $p > 0.05$). H, I: Exemplary recording of VB neurons before (H) and after (I) treatment with 10 µM spadin. In both cases, a depolarizing current step of +120 pA was applied. J: Input-output curve of VB neurons in wt C57BL/6J mice before and after application of 10 µM spadin (Mixed-effects analysis with Šidák correction, F (1, 8) = 2.538^{-5}, n = 5, $p > 0.05$). Abbreviations: AP, action potential; ctrl, control; I, current; ms, milliseconds; mV, millivolt; ns, not significant; pA, picoampere; RMP, resting membrane potential; SEM, standard error of the mean; t, time; TREK1, TWIK-related potassium channel 1; V, voltage; VB, ventrobasal thalamic complex; wt, wild type.

dose-dependent decrease of the I_{SO} in wt C57BL/6J mice. Mean sensitive currents were calculated for experiments with 1 µM (Figure 4G, reversal potential at −80 mV) and 10 µM (Figure 4I, reversal potential at −100 mV) of spadin in wt C57BL/6J mice. The resulting currents revealed a clear dose-depended effect on the I_{SO}.

Influence of BL-1249 and spadin on neuronal excitability

It has been described previously that pharmacological modulation of TREK1 impacts the neuronal resting membrane potential and thereby neuronal excitability (Bista et al. 2015b).

To investigate, whether BL-1249 and spadin influence neuronal excitability by either activating or blocking TREK1, we studied these substances in current-clamp experiments in VB neurons of wt C57BL/6J mice. A current step protocol was applied that gradually depolarized neurons (Figure 5A). For each current step, the number of APs during a 2.5 s test current injection (AP/2.5 s) was counted before and upon application of the respective compound and subsequently AP/2.5 s was plotted against the injected current to generate an input-output curve.

BL-1249 was tested at a concentration of 10 µM. Figure 5B, C shows exemplary recordings of neurons before and after treatment with BL-1249 illustrating the suppression of AP/2.5 s by BL-1249 (260 pA depolarizing current). The decrease in generation of AP/2.5 s was also detected in the input-output curve: Under control conditions, neurons generated a maximum number of 94.2 ± 8 AP/2.5 s. After BL-1249 was applied, this number was reduced to 89.6 ± 11.4 AP/2.5 s (Figure 5D, $p > 0.05$).

We also performed current-clamp experiments with spadin applied at concentrations of 1 µM and 10 µM. Comparing exemplary traces of neuron recordings before and after the treatment with 1 µM spadin (Figure 5E, F), suggested a mild increase in the number of APs upon application of spadin. However, the effect on AP/2.5 s was not significant (Figure 5G, $p > 0.05$).

By increasing the concentration of spadin to 10 µM, a trend for an increase in neuronal excitability was observed for step depolarizations between about +80 and +220 pA. This effect was evident for exemplary traces (Figure 5H, I) and in input-output curves (Figure 5J) – albeit not significant. Here, 10 µM spadin increased the number of generated AP/2.5 s up to a current injection of 260 pA. If more current was injected, cells started to show a depolarization block and the number of APs decreased compared to control conditions (130.6 ± 40.3 AP/2.5 s (spadin) versus 157.2 ± 38.2 AP/2.5 s (ctrl), $p > 0.05$). This phenomenon was not observed in untreated cells.

Whole-cell voltage-clamp recordings with the newly identified TREK1 activator A2: evaluation of TREK1 activation on neuronal cell population

Possible CNS side effects might be a potential roadblock to applying TREK1 activators *in vivo*. To provide further data on the effect of TREK1 activators on neurons, we performed a series of voltage-clamp experiments on murine VB neurons treated with A2. The same voltage-clamp ramp protocol as for BL-1249 and spadin was applied (Figure 6A) and the relative change of the I_{SO} was calculated.

First, we tested A2 at concentrations of 1, 10 (EC_{50}) and 100 µM in VB neurons of wt C57BL/6J mice. Against expectations, we observed a trend–albeit not significant–for a decrease of the I_{SO} (Figure 6B, $p > 0.05$). To investigate whether these findings are due to an interaction of A2 with TREK1, we tested treatment effects of 10 µM A2 in thalamic reticular nucleus (NRT) neurons that are known to have high TREK1 channel expression (Bista et al. 2015a) of wt C57BL/6J mice and in VB neurons of TREK1$^{-/-}$ mice. Again, we found a slight reduction of the I_{SO} amplitude by 4.0 ± 1.5% in wt NRT neurons and by 7.4 ± 1.3% in VB neurons of TREK1$^{-/-}$ mice (Figure 6C, $p > 0.05$). Figure 6D–F shows exemplary traces of recordings of wt VB and NRT neurons next to VB neurons of TREK1$^{-/-}$ mice, all treated with 10 µM A2. In all three examples, a decrease of the I_{SO} was seen. Corresponding mean sensitive currents were calculated and are displayed in Figure 6G–I. The resulting I-V relationships revealed some properties of K_{2P} channel carried outward rectification and a reversal close to the calculated K^+ equilibrium potential of –103 mV (Bista et al. 2015b, 2012; Meuth et al. 2003). However, especially in VB neurons a clear inwardly rectifying component was evident (Figures 6C, I).

Expression levels of TREK1 and TWIK-related potassium channel 2 (TREK2) in the murine brain

To further validate patch-clamp results, we studied the expression of TREK1 in different brain regions by semi-quantitative polymerase chain reaction (qPCR). All data are presented as $2^{-\Delta\Delta Ct}$ values depicting relative expression levels. All expression levels were normalized to those in the hippocampus.

TREK1 expression was confirmed in all brain regions investigated (Figure 7A). The highest expression levels were found in the primary somatosensory cortex (S1; 1.95 ± 0.5) followed by the cerebellum (0.95 ± 0.2). TREK1 was also expressed in the VB and NRT thereby corroborating the patch-clamp experiments shown above.

It has been previously described that BL-1249 not only activates TREK1 but also TREK2 (Pope et al. 2018). Therefore, we determined expression levels of TREK2 both in wt (Figure 7B) and in TREK1$^{-/-}$ mice (Figure 7C). In both cases, TREK2 showed a similar expression. The highest expression could be found in the cerebellum (16 ± 4 in wt C57BL/6J, 25.4 ± 7 in TREK1$^{-/-}$), followed by the NRT, VB and the S1.

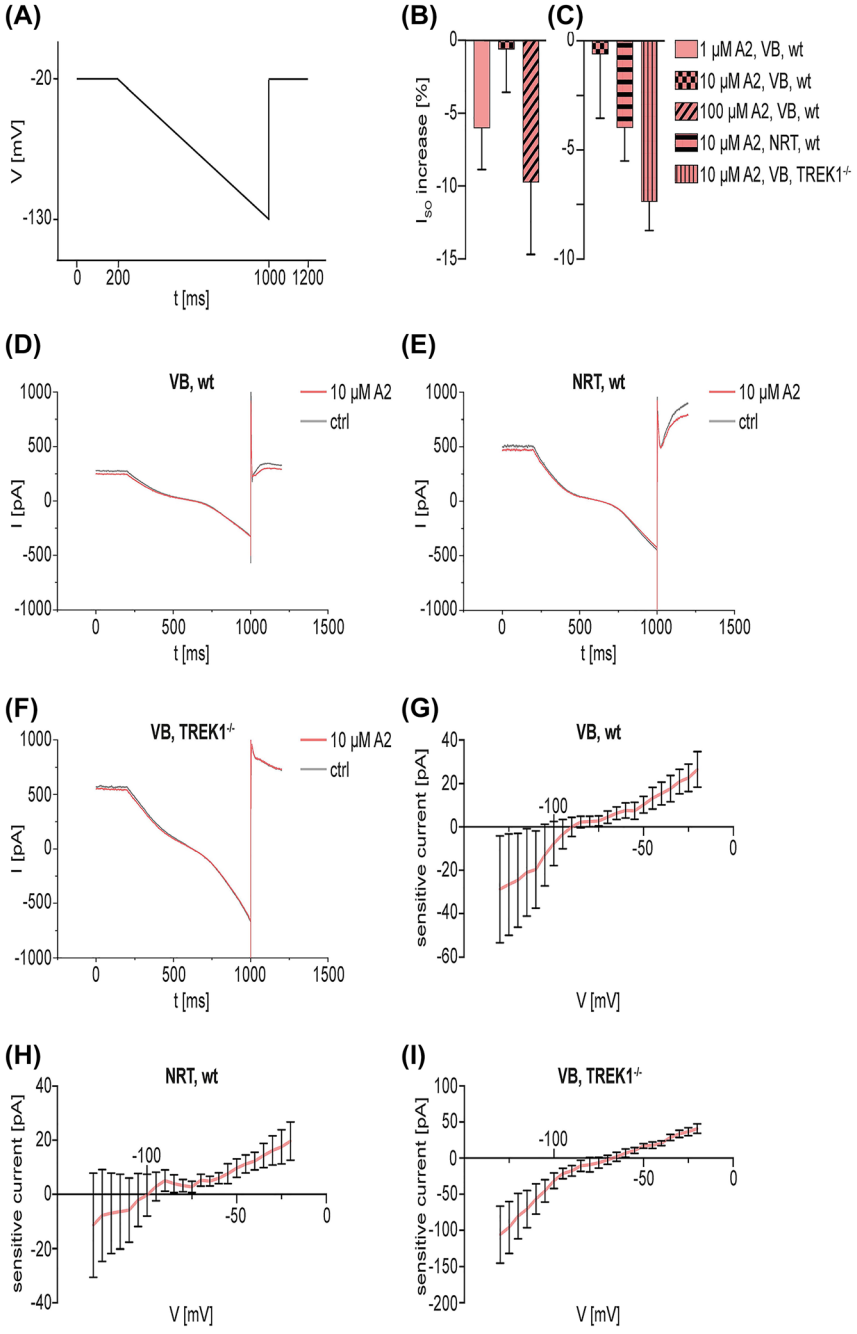

Figure 6: Whole-cell voltage-clamp recordings in murine VB and NRT neurons in wt C57BL/6J and TREK1$^{-/-}$ mice after treatment with the newly identified TREK1 activator A2. A: Ramp protocol used for voltage-clamp experiments. Cells were first held at −20 mV for 200 ms, then hyperpolarized to −130 mV over 800 ms, followed by another step at −20 mV for 200 ms. B: Effect of different A2 concentrations on the I_{SO} in wt C57BL/6J mice. The I_{SO} was measured before and after the TREK1 activator was washed into the external bath solution and its decrease [%] was calculated. A2 was tested in concentrations of 1, 10 and 100 µM (Kruskal–Wallis test including Dunn´s post-hoc test, n = 5–1 µM, n = 9–10 µM, n = 5–100 µM, $p > 0.05$). C: Measurements with 10 µM A2 in VB and NRT neurons in wt C57BL/6J mice and in VB neurons in TREK1$^{-/-}$ mice. The change of the I_{SO} [%] is depicted (Kruskal–Wallis test including Dunn´s post-hoc test, n = 9 - VB neurons in wt C57BL/6J mice, n = 5 - NRT neurons in wt C57BL/6J mice, n = 4 - VB neurons in TREK1$^{-/-}$ mice, $p > 0.05$). D, E, F: Exemplary recordings of murine neurons before (grey trace) and after (red trace) the treatment with 10 µM A2. Measurements were performed in VB neurons (D) and NRT neurons (E) in wt C57BL/6J mice as well as in VB neurons in TREK1$^{-/-}$ mice (F). G, H, I: Mean sensitive currents of voltage-clamp recordings after treatment with 10 µM A2. Measurements were performed in wt VB (G) and NRT neurons (H) as well as in VB neurons in TREK1$^{-/-}$ mice (I). Sensitive currents were calculated by graphically subtracting the currents before and after the substance was washed in. Abbreviations: Ctrl, control; I, current; I_{SO}, standing outward current; ms, milliseconds; mV, millivolt; NRT, thalamic reticular nucleus; pA, picoampere; SEM, standard error of the mean; t, time; TREK1, TWIK-related potassium channel 1; TREK1$^{-/-}$, TREK1 knockout; V, voltage; VB, ventrobasal thalamic complex; wt, wild type.

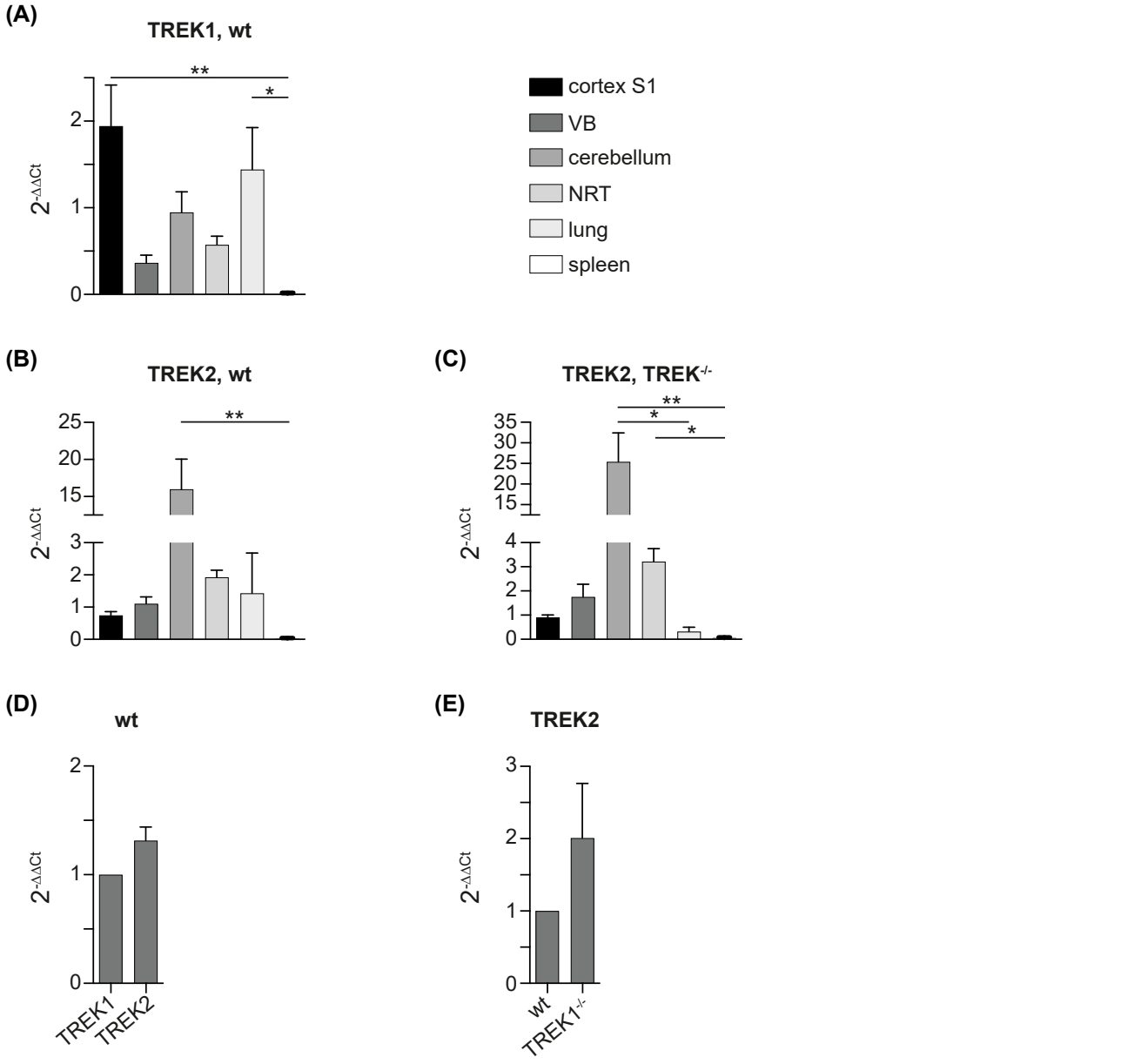

Figure 7: RT-qPCR showing the expression levels of TREK1 and TREK2 in different brain regions in wt C57BL/6J and TREK1$^{-/-}$ mice. Tissue was collected from the primary somatosensory cortex (S1), VB, cerebellum, NRT and hippocampus. The lung served as positive control, the spleen as negative control. After determination of the ΔCt values the $2^{-\Delta\Delta Ct}$ value was calculated to show relative expression levels. A: Relative expression of TREK1 in different brain regions in wt C57BL/6J mice. Expression levels were normalized to expression levels of the hippocampus. Hippocampal expression is therefore not shown (Kruskal–Wallis test including Dunn´s post-hoc test, $n = 4$, $p = 0.048$ for cortex S1 vs. spleen, $p = 0.029$ for lung vs. spleen, $p > 0.05$ for remaining data). B: Relative expression of TREK2 in different brain regions of wt C57BL/6J mice. Expression levels were normalized to those of the hippocampus (Kruskal–Wallis test including Dunn´s post-test, $n = 4$, $p = 0.0018$ for cerebellum vs. spleen, $p > 0.05$ for the remaining data). C: Relative expression of TREK2 in different brain regions of TREK1$^{-/-}$ mice. Expression levels were normalized to the hippocampus. (Kruskal–Wallis test including Dunn´s post-test, $n = 4$, $p = 0.0206$ for cerebellum vs. lung, $p = 0.0014$ for cerebellum vs. spleen, $p = 0.0477$ for NRT vs. spleen, $p > 0.05$ for the remaining data). D: Relative expression of TREK2 in comparison to TREK1 in the VB of wt C57BL/6J mice (One sample Wilcoxon test, $n = 4$, $p > 0.05$). E: Relative expression of TREK2 in VB neurons of TREK1$^{-/-}$ mice normalized to wt C57BL/6J mice (One sample Wilcoxon test, $n = 4$, $p > 0.05$). Abbreviations: Ct, cycle threshold; NRT, thalamic reticular nucleus; RT-qPCR, real-time polymerase chain reaction; S1, primary somatosensory cortex; SEM, standard error of the mean; TREK1, TWIK-related potassium channel 1; TREK1$^{-/-}$, TREK1 knockout; TREK2, TWIK-related potassium channel 2; VB, ventrobasal thalamic complex; wt, wild type.

Comparing the expression of TREK2 to the expression of TREK1 in wt VB neurons suggested a higher expression of TREK2 although not reaching significance (Figure 7D, $p > 0.05$).

Finally, we compared TREK2 expression levels in the VB of TREK1$^{-/-}$ mice to wt C57BL/6J mice (Figure 7E). Here, an upregulation of TREK2 in TREK1$^{-/-}$ mice was indicated–albeit not significant (2 ± 0.8 in TREK1$^{-/-}$ normalized to wt C57BL/6J, $p > 0.05$).

Discussion

Modulation of K_{2P} channels has emerged as a novel field of therapeutic strategies. Here, we report the identification of new TREK1 activators using an HTS. This approach yielded three substances, A2, B3 and E1, that activate TREK1 and inhibit TRESK K_{2P} channels. Functionally, we demonstrate that these compounds reduce the level of adhesion molecules on primary human endothelial cells. Cell viability was not affected. Finally, we studied A2 in detail as this compound displayed the smallest interaction potential with TRESK channels and the strongest effect on levels of adhesion molecules. Nonetheless, it should be noted that all compounds had an inhibitory effect on TRESK. Electrophysiological measurements showed that A2 had no significant effect on I_{SO} in native neurons. TREK channels carry about 5–10% of I_{SO} in thalamic neurons (Bista et al. 2015a). Comparison of voltage-clamp results in VB and NRT neurons, with the latter showing higher TREK1 expression levels, as well as TREK1$^{-/-}$ confirmed that A2 is not acting as specific TREK1 modulator in these native cells.

TREK1 has gained considerable interest as pharmacological target. In pathological conditions, such as chronic inflammation, TREK1 function might prove deleterious. In response to inflammatory signals, such as TNF-α, TREK1 is downregulated in brain ECs as well as epithelial and ECs of mucosal layers (Fang et al. 2019, 2017; Zyrianova et al. 2020). This data indicates TREK1 as regulator of immune cell response. Indeed, recent studies demonstrated that TREK1 modulates barrier functions. In mice, TREK1 inhibition or deficiency results in BBB leakage and increased leukocyte migration in EAE, but also following intracerebral hemorrhage or spinal cord injury (Bittner et al. 2013; Fang et al. 2019, 2017). Consequently, it is tempting to speculate that a specific TREK1- activator might dampen immune cell migration following inflammatory conditions. While TRE-K1 modulation might constitute a novel treatment target, potentially adverse effects must be considered first. Albeit limited to murine data, TREK1 knockout mice do not display differences in brain morphology, hippocampal development or general locomotion and behavior (Heurteaux et al. 2006). Further, neuronal cell lines, astrocytes and microglia appeared normal in TREK1 knockout mice (Zheng et al. 2022). Data in humans is sparse. However, analysis of sulcal openings as measured by magnetic resonance imaging in a retrospective study of ~15,000 individuals identified new loci associated with cortical volumes (Le Guen et al. 2019). Among these, TREK1 (*KCNK2*) was the single most influential variant implicated in cortical shrinking (Le Guen et al. 2019). Following this line of argumentation, it is important to note that the function of TREK1 is not limited to regulation of inflammatory mechanisms. One example is constituted by depression. In mice, TREK1 deletion results in a depression-resistant phenotype across 5 different murine models. This phenotype is also characterized by increased efficacy of 5-hydroxytryptamine signaling (Heurteaux et al. 2006). This data is corroborated in humans as TREK1 single nucleotide polymorphisms (SNPs) were associated with a more beneficial response to anti-depressants (Perlis et al. 2008). Interestingly, on a functional level, these TREK1 alleles were associated with an enhanced basal ganglia response to gains obtained in a reward/penalty test performed in healthy subjects (Dillon et al. 2009). Currently, novel small molecules, such as ML335, ML67-33, BL-1249 and compounds identified by HTS, as reported in our study, allow for pharmacological modulation of TREK1. Taken together, TREK1 modulation constitutes a tempting mechanism to regulate immune cell migration in inflammatory conditions. However, caution is warranted when translating these findings into humans as potential adverse effects may currently be insufficiently understood (Huntemann et al. 2022).

In a previous work, Bagriantsev et al. (2013) applied HTS to a library of 106 281 small molecules (Bagriantsev et al. 2013). This approach identified two inhibitors and three activators of TREK1, most notably the novel TREK1 activator ML67-33 (Bagriantsev et al. 2013). Similar to the compounds identified in our screening approach, ML67-33 is not specific for TREK1 but also acts on closely related K_{2P} and Ca^{2+}-activated BK-type channels (Schewe et al. 2019). Further, functional assays evaluating the biological activity of ML67-33 are currently lacking. Besides ML67-33, pharmacological profiling was previously applied to TREK1 resulting in identification of a novel group of small molecule TREK1 activators. These compounds, termed ML335 and ML402, act on TREK channels by stabilizing the C-type gate directly (Lolicato et al. 2017). In contrast to A2, B3 and E1 identified in our study, ML335 is specific for TREK1 and TREK2 with only negligible effects on TRESK (Lolicato et al. 2017). Notably, in our hands ML335 has a stronger inhibitory effect on TRESK channels and compound A2 of our screening approach also

activates TREK2 channels to the same degree like TREK1 comparable to ML335 (Supplementary Figure 2). However, together with our current work, HTS appears as a suitable strategy to identify novel TREK1 modulators providing the groundwork for future studies to better understand the influence of TREK1 in health and disease.

Our understanding of TREK1 modulation might be enhanced by the gene expression data presented in our study. Here, we report that the primary somatosensory cortex expressed the highest level of TREK1, while TREK2 is mostly expressed in the cerebellum. Interestingly, TREK2 expression was detected in wt and TREK1$^{-/-}$ mice. These observations are in line with previous studies in rat observing TREK1 expression in the CNS and spinal cord (Hervieu et al. 2001). Studies employing high-resolution techniques such as single cell transcriptomics might be a valuable tool to further improve our understanding of the cell specific TREK1 architecture in the brain.

The scope of this work is limited to an *in vitro* study of potential TREK1 modulators. Follow-up studies are needed to demonstrate an effect of these substances *in vivo*. The established murine EAE model might be a feasible choice for such studies. Furthermore, while we observed comparable effects of E1, B3 and A2 to BL-1249 - an established TREK1 activator–in functional transmigration assays, future experiments might be improved by incorporating a negative control to better quantify the substances individual effectivity. Concurrently, the reader should be mindful that potentially off-target effects are superimposed on the results observed in this study. In order to assess the effect of TREK1 modulators on currents in native neurons, the results of the present study may indicate the use of neurons with strong expression, like cerebellar cells. Finally, we chose a supra-physiological dose of BL-1249 for HTS. Future studies might benefit from incorporating different dosing regimens for HTS testing.

Taken together, this study provides data on novel TREK1 activators that might be employed to pharmacologically modulate TREK1 activity in neuroinflammation.

Materials and methods

Origin of tested TREK1 activators

The 104 192 substances for initial HTS experiments as well as the three final selected compounds were purchased from the Enamine® substance library (https://enamine.net; Enamine, Kiev, Ukraine): E1 (#Z220539848), B3 (#Z27879940) and A2 (#Z56776203). For downstream assays, EC_{50} concentrations were used.

Mice

C57BL/6J wt mice (Envigo, Horst, the Netherlands) were housed under specific pathogen-free conditions in individually ventilated cages (IVC) with 55–65% humidity at 24 ± 2 °C with a 12 h light/dark cycle and had access to food and water *ad libitum*. TREK1$^{-/-}$ mice with a C57BL/6J genetic background were kindly provided by Heurteaux et al. (Heurteaux et al. 2004).

Transfection of HEK293T cells with TREK1

The HEK239T cell line was generated as described in (Moha ou Maati et al. 2011). Briefly, the hTREK1 (pIRES2-eGFP) vector was transfected into HEK293T cells in the presence of 1.5 mg/mL geneticin. Geneticin resistant clones were collected and cultivated after three to four weeks. Cells were cultivated for a total of 14 passages. TREK1 expression was confirmed by qPCR and cells were used for subsequent experiments.

FluxOR™ assay

HEK293T cells stably transfected with human TREK1 were seeded the day before the assay readout at 20,000 cells/well in Dulbecco's Modified Eagles Medium (DMEM)-media containing 1% FCS, 1% Gln, 1% Pen/Strep/G418. Cells were incubated for 20 h at 37 °C in humid atmosphere and 5% CO_2. On the day of the assay, cells were removed from the incubator and loaded with the FluxOR™ dye, followed by 1 h incubation at RT. The dye mixture contained: the Powerload concentrate 1:50, FluxOR Dye 1:1500, FluxOR Assay Buffer rest (FluxOR assay buffer component B 1:10, HEPES (1 M) 1:50, pH 7,4, H_2O), Probenecid 1:40 and the BackDrop Reagent 1:4. All components despite the HEPES buffer and the BackDrop Reagent (BackDrop™ Background Suppressor for Microplate Assays, Invitrogen™, #B10512) are provided in the kit (FluxOR™ Potassium Ion Channel Assay, Invitrogen™, #F10016). By the end of incubation time compounds/DMSO were added to the respective well (maximum 0.25% v/v DMSO i.a.) followed by additional 20 min incubation at RT. Signal of dye-loaded cells was detected on the Envision HTS microplate reader (PerkinElmer) using the bottom readout and FITC 485/FITC 535 filter settings. Thallium (Tl_2SO_4) was added to cells using 0.85 mM Tl^+ i.a., the assay plate was immediately read on the Envision HTS microplate reader. The signal was calculated as relative fluorescence unit ratio (RFU-ratio) of the signal detected after thallium addition to pre-thallium addition signal. The assay was optimized regarding cell number, DMSO tolerance, and response to known TREK1 activators.

Screening

Enamine compound collection was selected for screening. It includes low molecular weight organic compounds as well as diverse drug-like compounds, among them ~70 K predominately 'lead-like' compounds with potential activity against relatively well-defined target classes (type I GPCRs, kinases, ion channels, proteinases etc.); ~30 K compounds against less well-defined targets (especially protein-protein interactors) and 100 K diverse, predominantly 'lead-like' structures.

For primary screening, test compounds (stock at 2 mM in 100% DMSO), positive (BL-1249 25 mM in 100% DMSO) and negative (100%

DMSO) controls, were transferred to 384-well assay microplates (Corning® #3764) by acoustic dispensing (Echo, Labcyte). Plate concentrations were: test compounds at 10 µM (columns 1 to 22); positive control 125 µM (column 23) and negative control DMSO 0.5 %v/v (column 24). Assay was performed as described above using optimized conditions.

Z' calculation was used for assessment of quality of screened plates (Zhang et al. 1999). The Z′ value represents a reference value for a screening assay, it's calculated according to the average signal and standard deviation of the positive and negative controls. All calculated values > 0.5 show a suitable assay for screening.

$$Z' = 1 - \frac{3*(SD_{high} + SD_{low})}{AV_{high} - AV_{low}}$$

Data were analyzed using ActivityBase (idbs). Plates with $Z' < 0.5$ were rejected and repeated.

Cytotoxicity

Cytotoxicity assessment of test compounds was performed using the Promega CellTiter-Glo (#G7570) assay kit. Compounds were incubated at increasing concentrations with cells to determine the half maximum concentration needed to reduce cell viability to 50% (CC_{50}). The assay is based on measurement of the intracellular ATP level as a marker for metabolic active cells. HEK293T/TREK1 cells, grown in DMEM with 10% fetal bovine serum, L-Glutamine, streptomycin, and 100 U/mL penicillin and G418 were seeded into white 384-well microtiter plates (Greiner Bio-One, #781073) at 8000 cells/20 µL/well and incubated at 37 °C in the presence of 5% CO_2 for 24 h. Compounds (100 nL of 2 mM stock concentration in 100% v/v DMSO) and controls (TNF-α 100 nL/well of 0.1 mg/mL stock concentration in 100% v/v DMSO, and 100 nL/well of 100% v/v DMSO (Carl Roth, #HN47.1)) were added to cells using the Echo 550 Liquid Handler and incubated for 48 h at 37 °C in the presence of 5% CO_2. ATP was detected using 10 µL of the CellTiter-Glo Detection Reagent added to each well, the microplate was incubated in the dark for 15 min. The generated luminescence signal was detected using the EnVision Multilabel 2103 Reader with 10 ms reading time/well. Data analysis was performed using Microsoft Excel and GraphPad Prism. Test compound results were normalized relative to DMSO control representing 0% inhibition of cell viability and TNF-α control representing 100% inhibition of cell viability.

Electrophysiological measurements of *Xenopus laevis* oocytes and HEK293T cells

Molecular biology and expression: For this study we used the coding sequences of WT hTWIK-1 (GenBank accession number: NM_002,245.3), hTWIK-2 (EU978937.1), hTREK-1 (NM_172,042.2), hTREK-2 (NM_138,318.2), hTRAAK (AF_247,042.1), hTASK-2 (NM_003,740.3), hTALK-1 (NM_032,115.4), hTALK-2 (EU978944.1), hTASK-1 (NM_002,246.2), hTASK-3 (XM_011,517,102.1), hTHIK-1 (NM_022,054), hTHIK-2 (NM_022,055.1) and hTRESK (NM_181,840.1). To increase surface expression and macroscopic currents, measurements of TWIK-1, TWIK-2 and THIK-2 channels were done using channels with mutated retention motifs and an additional point mutation in hTHIK-2, respectively (TWIK-1 I293A/I294A (TWIK-1*) (TWIK-2 I289A/L290A) (TWIK-2*) and THIK-2 R11A/R12A/R14A/R15A/R16A/A155P (THIK-2*)). WT constructs were subcloned into the pFAW dual purpose vector suitable for *in vitro* transcription/oocyte expression and transfection of cultured cells and verified by sequencing. cRNA was synthetized using AmpliCap-Max T7 or SP6 High Yield Message Maker Kits (Cellscript, USA) and stored at −20 °C (for frequent use) or −80 °C (for long term storage).

Animals (*X. laevis*) and cell culture: *X. laevis* oocytes were surgically removed from adult female frogs and treated with type II collagenase prior to manual defolliculation. Oocytes were incubated at RT for 60–75 min with 2 µg/mL collagenase type II (Biochrom GmbH, Berlin) solved in OR2 solution. The performed investigation conforms to the guide for the Care and Use of Laboratory Animals (NIH Publication 85–23). For this study, we used female *X. laevis* animals that were accommodated at the animal breeding facility of the Christian-Albrechts-University of Kiel to isolate oocytes. Experiments using *X. laevis* were approved by the local ethics commission. Oocytes were injected with ~50 nL of channel-specific cRNA (0.5–1 µg/µL) and incubated at 16.9 °C for one to four days prior to experimental use.

Stably transfected human HEK293T/TREK1 cells were cultured in DMEM supplemented with 10% (vol/vol) heat-inactivated FCS and 10 U/mL penicillin, 10 mg/mL streptomycin and 1 µg/mL puromycin in an atmosphere of 95% air and 5% CO_2 at 37 °C. For electrophysiological recordings, the transfected cells were trypsinized at least 2 h before electrophysiological measurements and incubated in external recording buffer.

Inside-out patch-clamp recordings of *Xenopus* oocytes: Macroscopic currents were recorded from inside-out membrane patches excised from cRNA-injected *Xenopus* oocytes at RT (21–23 °C). Pipettes were made from thick-walled borosilicate glass capillaries and had resistances of 0.3–0.5 MΩ. Pipettes were filled with a standard pipette solution (in mM): 120 KCL, 10 HEPES and 3.6 $CaCl_2$, pH 7.4 was adjusted with KOH/HCl. Currents were recorded using an EPC10 amplifier (HEKA electronics), sampled at 10 kHz and filtered with 3 kHz (−3 dB). The recording program was Patchmaster (HEKA electronics, version: v2x73.5, Lamprecht, Germany). The used pulse protocols were either ramps ranging from −80 to +80 mV with a duration of 1 s and a pulse interval of 9 s, or measurements were carried out using a continuous pulse at −80 mV. Solutions were applied to the cytoplasmic side of excised membrane patches via a gravity-flow multi-barrel application system. Standard intracellular (bath) solutions were composed of (in mM): 120 KCl, 10 HEPES, 2 EGTA and 1 pyrophosphate. pH was adjusted to pH 7.4 or 5.0 with KOH/HCl.

Whole-cell recordings of HEK293T cells: HEK293T cell measurements were done in the whole-cell configuration of the automated patch-clamp technique using a Port-a-Patch mini/PatchControl mini software (Nanion Technologies, Munich, Germany), sampled at 10 kHz and filtered with 3 kHz. Pipette resistances ranged from 2 – 3.5 MΩ. Intracellular (internal) potassium solution KF110 (mM): 110 KF, 10 KCl, 10 NaCl, 10 EGTA and 10 HEPES. The internal solution was set to a pH of 7.2 with KOH/HCl and an osmolarity of 295 mOsm kg^{-1}. The extracellular (external) solution contained (mM): 140 NaCl, 4 KCl, 1 $MgCl_2$, 2 $CaCl_2$, D-Glucose monohydrate and 10 HEPES. The external solution was set to a pH of 7.4 with NaOH/HCl and the osmolarity was set to 298 mOsm kg^{-1}.

TREK1 currents were elicited by 900 ms ramps from −120 to +60 mV applied from a holding potential (VH) of −80 mV with 3.5 s interpulse intervals and analyzed at +40 mV. TREK1 activation was carried out with 125 µM BL-1249 in the external solution. BL-1249 was dissolved in DMSO as 50 mM stock and stored at −20 °C prior to experiments. While recording, BL-1249 was diluted in the external solution to the final concentration and applied via a three times repeated exchange of the total external solution volume. Control applications with the same vehicle concentration of DMSO without BL-1249 were measured with the respective cells.

Chemical compounds

Stock solutions of respective substances were prepared in DMSO (10–20 mM). Stock solutions were stored at −80 °C and diluted in the bath solution to the final concentration prior to measurements. Tetra-Pentyl-Ammonium chloride (TPenA) and BL-1249 were purchased from Sigma-Aldrich/Merck (Darmstadt, Germany) and stock solutions were prepared in DMSO (50–100 mM). TPenA was used to test for patch integrity (1 mM TPenA exhibited almost full block of channel-specific current) in each measurement.

Data analysis

Data analysis was performed using Fitmaster (HEKA electronics, version: v2x73.5, Lamprecht, Germany), PatchControl mini software (Nanion Technologies, Munich, Germany), Microsoft Excel (Microsoft Corporation, version: Microsoft Office Professionel Plus 2019, Redmond, USA) and Igor Pro (Wavemetrics Inc., version: 6.3.7.2, Portland, USA). Recorded currents were analyzed from stable membrane patches at a voltage of −80 mV or stable HEK cells at +40 mV. The fold activation of a ligand (substance) was calculated from the following equation:

$$\text{Fold activation (FA)} = \frac{I_{activated}}{I_{basal}}$$

with $I_{activated}$ representing the maximum current level in the presence of a given concentration of a respective substance and I_{basal} the measured current before compound application.

Percentage inhibition of a substance was calculated from stable currents of excised membrane patches using the following equation below:

$$\%\ \text{inhibition} = \left(1 - \left(\frac{I_{inhibited}}{I_{basal}}\right)\right)*100$$

where $I_{inhibited}$ refers to the minimum current level recorded in the presence of a given concentration of a compound and I_{basal} to the measured current before ligand application.

The macroscopic half-maximal concentration-inhibition relationship of a substance was obtained using a modified Hill-equation depicted below:

$$\frac{I}{I_{basal}} = a + \frac{(1-a)\left(\frac{[x]}{IC_{50}}\right)^{h}}{1 + \frac{[x]}{IC_{50}}h}$$

with I and I_{basal} representing the currents in the absence and presence of a respective compound, x is the concentration of the compound, IC_{50} is the ligand concentration at which the inhibitory effect is half maximal, h is the hill coefficient and a is the fraction of inert current ($a = 0$). Inside-out patch-clamp and whole-cell data are represented as mean ± SEM (standard error of the mean).

Isolation, purification and cultivation of primary human cells

Muscle tissue was dissociated using a muscle dissociation kit from Miltenyi Biotech (Germany) and a gentleMACS dissociator. For PHMCs, we used a CD56-PE (clone N901, Beckman Coulter) antibody combined with PE microbead magnetic separation. Biolaminin 521 LN coated 6-well plates and skeletal muscle cell growth medium from PELO Biotech were used for cultivation according to the manufacturer's instructions. For all experiments, we used differentiated PMHCs by growing cells over 90% confluence and changing growth to differentiation medium (basal media with 2% horse serum and antibiotic, without growth factors, FCS or cortisol). For PHMEC purification, we depleted $CD45^+$ and enriched $CD31^+$ cells by using magnetic microbeads from Miltenyi Biotech (Germany). A microvascular endothelial cell growth medium (PELO Biotech) on collagen based coated 6-well plates was used for cultivation until cells reached a confluent monolayer.

Flow cytometry analysis

Flow cytometry was used to analyze level of surface markers on PHMCs and PHMECs. Here, PHMCs and PHMECs were treated with TNF-α (500 U/mL) over 24 h. After stimulation, cells were washed and fresh medium was applied. Additionally, ECs were treated with or without EC_{50} concentrations of K_{2P} modulators (BL-1249 - 10 µM, Spadin – 1 µM, A2 – 8.56 µM, B3 – 5.86 µM, E1 – 16.84 µM). To analyze inflammatory cell response, the following antibodies were used: HLA A, B, C (FITC, W6/32), HLA-DR (APC, L243), CD54 (PB, HA58), CD31 (AF700, WM59), CD106 (APC, STA). PBMC: CD11b (FITC, ICRF44), CD56 (PerCP/Cy5.5, B159), CD3 (PE Cy7, SP34-2), CD11c (APC, SHCL3), CD20 (AF700, 2HF), CD4 (APC/Cy7, SK3), CD8a (PB, HIT8a).

Adhesion assay

PHMECs (6×10^4 cells per chamber) were seeded in an ibidi® µ-slides IV 0.4 coated with speed coating solution (PELO Biotech). Cells were cultivated for at least 48 h in microvascular endothelial cell growth media (PELO Biotech) until reaching confluence. Cells were left untreated for 24 h (0–24 h). Then, cells were treated with TNF-α 500 U/mL for another 24 h (24–48 h). After wash-out, cells were left untreated for 24 h (48–72 h). Cells were treated with 1% DMSO, BL-1249 or testing compounds as described in the corresponding section. Stimulated PBMCs were added to PHMECs, respectively. Adhesion of immune cells was quantified with a Zeiss Axiovert A.1 microscope detecting bright-field images in a time series (1 image per 10 s for 30 min) under flow conditions (a flow rate of 0.25 dyn/cm^2). Immune cells were perfused by using a pump system. After 30 min the amount of adhered immune cells were analyzed by cell counting plugin from ImageJ.

Transmigration assay

To test the transmigratory capacity of T cells, we performed a transmigration assay with minor modifications as described in (Bittner et al. 2013). PHMECs (6×10^4 cells) were seeded in a coated (Speed coating solution, PELO Biotech) insert of a transwell and cultivated for 48 h with microvascular endothelial cell growth medium (PELO Biotech). Cells were inflamed as described above and treated with 1% DMSO, BL-1249 or test compounds. 5×10^5 stimulated PBMCs were added. After 8 h, we added Flow-Count Fluorosphere (Beckman Coulter) to the migrated cells from the lower compartment. Cells were labelled with antibodies (see

flow cytometry analysis) and relative cell counts were determined by flow cytometry.

Patch-clamp and voltage-clamp recordings in murine VB and NRT neurons

Preparation of brain slices for patch-clamp recordings: For the patch-clamp experiments, wt C57BL/6J and TREK1$^{-/-}$ mice in the age of 4–6 weeks were used. After anesthesia with isoflurane, mice were decapitated, and the brain was rapidly removed. Brains were then placed into a vibratome (Leica Biosystems, Wetzlar, Hessen, Germany), where coronal, thalamic brain slices with a thickness of 260 µm were fabricated. Inside the vibratome, the brains were submerged with an ice-cold cutting solution, that contained the following: KCl 2.5 mM; NaH_2PO_4 1.25 mM; $MgSO_4$ 10 mM; PIPES 20 mM; glucose 10 mM; sucrose 200 mM; $CaCl_2$ 0.5 mM; pH was set to 7.35 using NaOH (Sigma-Aldrich, St. Louis, Missouri, USA; Merck, Darmstadt, Hessen, Germany). The brain slices were then transferred into a custom-made holding chamber, where they were kept until used for patch-clamp experiments. The holding chamber contained the following solution: NaCl 125 mM; KCl 2.5 mM; NaH_2PO_4 1.25 mM; $MgSO_4$ 2 mM; $NaHCO_3$ 24 mM, glucose 10 mM; $CaCl_2$ 2 mM (Sigma-Aldrich; Merck). The solution was bubbled with carbogen gas (95% O_2, 5% CO_2) to set the pH to 7.35.

Patch-clamp recording settings: For the patch-clamp recordings, slices were placed into the setup, where they were continuously perfused with artificial cerebrospinal fluid (ACSF) at a rate of 1.5 mL/min. The ACSF solution contained the following: NaCl 120 mM; KCl 2.5 mM; NaH_2PO_4 1.25 mM; $NaHCO_3$ 22 mM; glucose 25 mM; $MgSO_4$ 2 mM; $CaCl_2$ 2 mM, the pH was set to 7.35 by bubbling the solution with carbogen gas. Thalamic neurons in the VB and the NRT were identified using a bright light microscopy (AX10 Examiner A1, Zeiss, Oberkochen, Baden-Württemberg, Germany). Pipettes were pulled from borosilicate glass (GC150TF-10, Warner Instruments, Holliston, MA, USA) using a vertical pipette puller. The pipettes were then filled with a solution containing NaCl 10 mM; K-gluconate 88 mM; K_3-citrate 20 mM; HEPES 10 mM; BAPTA 3 mM; phosphocreatine 15 mM; $MgCl_2$ 1 mM; $CaCl_2$ 0.5 mM; Mg-ATP 3 mM; Na-GTP 0.5 mM; pH set to 7.25 with KOH; the osmolarity was adjusted to 290–300 mOsmol/kg (Sigma–Aldrich; Merck). Pipettes were then connected to an EPC-10 amplifier (HEKA Elektronik, Lamprecht, Rhineland–Palatinate, Germany). Electrode resistance ranged from 4-8 MΩ. Electrophysiological experiments were controlled by the Patchmaster software (HEKA Elektronik). For all measurements, the substances were washed into the external bath solution during the recording. A liquid junction potential of 10 mV was measured; however, it is not considered in the data. All experiments were performed at RT.

Voltage-clamp experiments: For voltage-clamp experiments, Tetrodotoxin (Abcam, Cambridge, UK) at a concentration of 500 nM was added to the bath solution to block voltage-dependent Na^+ channels. After establishing the whole-cell configuration, a typical voltage step protocol for the study of K_{2P} channels was applied (Meuth et al. 2003; Millar et al. 2000). Cells were first held at –20 mV for 200 ms to inactivate voltage-dependent membrane currents and to increase the amplitude of currents carried by K_{2P} channels (Bista et al. 2015b). After that, neurons were hyperpolarized to –130 mV over 800 ms, followed by another step at –20 mV for 200 ms. For analysis of the effect of the substances the I_{SO} at –20 mV was measured before and after the substance was washed into the external bath solution and its relative increase in percent was calculated. Sensitive currents were calculated by graphically subtracting the currents before and after the substance was washed in.

Current-clamp experiments: To investigate, whether the compounds impact neuronal excitability, additional current-clamp experiments were performed. All current-clamp experiments were performed at RMP. From the RMP, a standard current step protocol (modified from (Zobeiri et al. 2018)) was applied with each step of the protocol increasing the current injected by 20 pA and lasting for 2.5 s. The current injected ranged from –180 pA to 420 pA. Afterwards, input-output curves were generated by plotting the number of APs generated against the injected current. APs were automatically counted using the Peak software (Meuth IT Consulting, Butzbach, Hessen, Germany).

Drugs: BL-1249 (Sigma-Aldrich), a known activator of TREK1 (Pope et al. 2018), was used as a positive control and was dissolved in DMSO. Spadin (Sigma Aldrich, for experiments with 1 µM; MedChemExpress, Monmouth Junction, NJ, USA, for experiments with 10 µM) was dissolved in water and used as a negative control (Mazella et al. 2010). The newly identified TREK1 activator A2 (Enamine) was dissolved in DMSO. If DMSO was used as a solvent, its concentration in the external bath solution did not exceed 1‰.

RT-qPCR analyses of TREK1 and TREK2 expression levels in the CNS

As for patch-clamp experiments, wt C57BL/6J and TREK1$^{-/-}$ mice at the age of 4–6 weeks were anesthetized with isoflurane and then decapitated. After removal of the brain, tissue from the S1, VB, cerebellum, NRT and hippocampus were collected. The lung and spleen were removed as well and served as positive (lung) and negative (spleen) controls, respectively. After mechanical homogenization, RNA was extracted by using Trizol reagent (Thermo Fisher, Waltham, MA, USA) according to standard procedures. Complementary DNA (cDNA) was synthesized using random hexamer primers (Thermo Fisher) with an amount of 500 ng RNA in a Labcycler Basic (Sensoquest, Göttingen, Germany) with the following protocol: 25 °C for 10 min, 50 °C for 30 min, 85 °C for 5 min.

qPCR experiments were performed in a StepOnePlus Real-Time PCR System (Thermo Fisher) with the Maxima Probe/ROX qPCR Master Mix (2x, Thermo Fisher). 18s RNA was used as endogenous control. Primers for TREK1 (Mm01323942_m1; Thermo Fisher) and TREK2 (Mm00504118_m1; Thermo Fisher) were used. 50 cycles of the following program were run: 50 °C 2 min, 95 °C 10 min, 95 °C 15 s, 60 °C, 1 min. Afterwards, delta values were determined between threshold cycles (ΔCT) of the gene of interest and the endogenous control. By normalizing the ΔCt values to a specific tissue, ΔΔCt values were generated, which are then shown as the $2^{-\Delta\Delta Ct}$ value to illustrate the relative quantification.

Statistical analysis

Results are displayed as means ± SEM unless indicated otherwise. For column-based data, Gaussian distribution was evaluated by D`Agostino-Pearson normality test. Dependent on normality for analysis of two groups, two-tailed *t*-test (unpaired/paired) or Mann–Whitney *U* test was used as appropriate. If more groups were compared, we applied One-way ANOVA, complemented by Bonferroni test for multiple

comparisons for parametric data, or the Kruskal–Wallis test including Dunn's post-test for non-parametric data.

The level of significance was labelled according to the *p*-values: p values > 0.05 were classified as not significant, $p < 0.05$ (*) as significant, $p < 0.01$ (**), $p < 0.001$ (***) and $p < 0.0001$ (****) as highly significant. Analyses and graphs were prepared using Prism 9.1.2 (Graph Pad, San Diego, CA, USA).

Visualization

Figures were created using Adobe Illustrator (version 2022) and Servier Medical Art (accessible at: https://smart.servier.com).

Acknowledgements: The authors thank Jeannette Budde for her excellent technical assistance.

Author contributions: Conceptualization: C.B.S., C.N., M.S., L.S., M.K., P.G., P.H., T.Ba., B.W., S.B., T.R., T.Bu. and S.G.M.; Data acquisition: C.B.S., C.N., M.S., L.S., T.M., M.K. and L.C.N.; Formal Analysis: C.B.S., C.N., M.S., L.S., T.M. and M.K.; Funding acquisition: S.G.M.; Resources: M.K., M.S., T.Ba., T.Bu. and S.G.M.; Supervision: T.Bu. and S.G.M.; Visualization: C.B.S., M.S., N.H. and M.K.; Writing–original draft: C.B.S., C.N., M.S., L.S. and M.K.; Writing–review & editing: M.S., A.M.H., T.M., N.H., P.G., S.A., S.B., P.H., L.C.N., T.Ba., G.S., B.W., S.B., T.R., T.Bu. and S.G.M.

Research funding: The project was funded by the Chembion DFG-graduate school (GKR 2515). M.S. and T.Ba. were supported by the Deutsche Forschungsgemeinschaft (DFG, German Research Foundation) as part of the Research Unit FOR2518, *DynIon*.

Conflict of interest statement: The authors declare no competing interests.

Data availability: The data sets generated and analysed during the current study are available from the corresponding author on reasonable request: Prof. Sven Meuth, Department of Neurology, Heinrich-Heine University Düsseldorf, Moorenstr. 5, D-40225 Düsseldorf, Germany, Phone: 0049 (0) 211-81-19532, meuth@uni-duesseldorf.de.

References

Afzali, A.M., Ruck, T., Herrmann, A.M., Iking, J., Sommer, C., Kleinschnitz, C., Preuβe, C., Stenzel, W., Budde, T., Wiendl, H., et al. (2016). The potassium channels TASK2 and TREK1 regulate functional differentiation of murine skeletal muscle cells. Am. J. Physiol. Cell Physiol. 311: C583–C595.

Bagriantsev, S.N., Ang, K.-H., Gallardo-Godoy, A., Clark, K.A., Arkin, M.R., Renslo, A.R., and Minor, D.L. (2013). A high-throughput functional screen identifies small molecule regulators of temperature- and mechano-sensitive K2P channels. ACS Chem. Biol. 8: 1841–1851.

Bista, P., Cerina, M., Ehling, P., Leist, M., Pape, H.-C., Meuth, S.G., and Budde, T. (2015a). The role of two-pore-domain background K^+ (K_2p) channels in the thalamus. Pflüger's Arch 467: 895–905.

Bista, P., Meuth, S.G., Kanyshkova, T., Cerina, M., Pawlowski, M., Ehling, P., Landgraf, P., Borsotto, M., Heurteaux, C., Pape, H.-C., et al. (2012). Identification of the muscarinic pathway underlying cessation of sleep-related burst activity in rat thalamocortical relay neurons. Pflüger's Arch 463: 89–102.

Bista, P., Pawlowski, M., Cerina, M., Ehling, P., Leist, M., Meuth, P., Aissaoui, A., Borsotto, M., Heurteaux, C., Decher, N., et al. (2015b). Differential phospholipase C-dependent modulation of TASK and TREK two-pore domain K^+ channels in rat thalamocortical relay neurons: PLC-dependent modulation of thalamic activity. J. Physiol. 593: 127–144.

Bittner, S., Ruck, T., Fernández-Orth, J., and Meuth, S.G. (2014). TREK-king the blood-brain-barrier. J. Neuroimmune Pharmacol. 9: 293–301.

Bittner, S., Ruck, T., Schuhmann, M.K., Herrmann, A.M., Maati, H.M., Bobak, N., Göbel, K., Langhauser, F., Stegner, D., Ehling, P., et al. (2013). Endothelial TWIK-related potassium channel-1 (TREK1) regulates immune-cell trafficking into the CNS. Nat. Med. 19: 1161–1165.

Dadi, P.K., Vierra, N.C., Days, E., Dickerson, M.T., Vinson, P.N., Weaver, C.D., and Jacobson, D.A. (2017). Selective small molecule activators of TREK-2 channels stimulate dorsal root ganglion c-fiber nociceptor two-pore-domain potassium channel currents and limit calcium influx. ACS Chem. Neurosci. 8: 558–568.

Decher, N., Rinné, S., Bedoya, M., Gonzalez, W., and Kiper, A.K. (2021). Molecular pharmacology of K2P potassium channels. Cell. Physiol. Biochem. 55: 87–107.

Dillon, D.G., Bogdan, R., Fagerness, J., Holmes, A.J., Perlis, R.H., and Pizzagalli, D.A. (2009). Variation in TREK1 gene linked to depression-resistant phenotype is associated with potentiated neural responses to rewards in humans. Hum. Brain Mapp. 31: 210–221.

Djillani, A., Mazella, J., Heurteaux, C., and Borsotto, M. (2019). Role of TREK-1 in health and disease, focus on the central nervous system. Front. Pharmacol. 10: 379.

Ehling, P., Cerina, M., Meuth, P., Kanyshkova, T., Bista, P., Coulon, P., Meuth, S.G., Pape, H.-C., and Budde, T. (2013). Ca^{2+}-dependent large conductance K^+ currents in thalamocortical relay neurons of different rat strains. Pflüger's Arch 465: 469–480.

Fang, Y., Huang, X., Wan, Y., Tian, H., Tian, Y., Wang, W., Zhu, S., and Xie, M. (2017). Deficiency of TREK-1 potassium channel exacerbates secondary injury following spinal cord injury in mice. J. Neurochem. 141: 236–246.

Fang, Y., Tian, Y., Huang, Q., Wan, Y., Xu, L., Wang, W., Pan, D., Zhu, S., and Xie, M. (2019). Deficiency of TREK-1 potassium channel exacerbates blood-brain barrier damage and neuroinflammation after intracerebral hemorrhage in mice. J. Neuroinflammation 16: 96.

Hervieu, G.J., Cluderay, J.E., Gray, C.W., Green, P.J., Ranson, J.L., Randall, A.D., and Meadows, H.J. (2001). Distribution and expression of TREK-1, a two-pore-domain potassium channel, in the adult rat CNS. Neuroscience 103: 899–919.

Heurteaux, C., Guy, N., Laigle, C., Blondeau, N., Duprat, F., Mazzuca, M., Lang-Lazdunski, L., Widmann, C., Zanzouri, M., Romey, G., et al. (2004). TREK-1, a K^+ channel involved in neuroprotection and general anesthesia. EMBO J. 23: 2684–2695.

Heurteaux, C., Lucas, G., Guy, N., El Yacoubi, M., Thümmler, S., Peng, X.-D., Noble, F., Blondeau, N., Widmann, C., Borsotto, M., et al. (2006). Deletion of the background potassium channel TREK-1 results in a depression-resistant phenotype. Nat. Neurosci. 9: 1134–1141.

Huntemann, N., Bittner, S., Bock, S., Meuth, S.G., and Ruck, T. (2022). Mini-review: two brothers in crime - the interplay of TRESK and TREK in human diseases. Neurosci. Lett. 769: 136376.

Lauritzen, I., Chemin, J., Honoré, E., Jodar, M., Guy, N., Lazdunski, M., and Jane Patel, A. (2005). Cross-talk between the mechano-gated K2P channel TREK-1 and the actin cytoskeleton. EMBO Rep. 6: 642–648.

Le Guen, Y., Philippe, C., Riviere, D., Lemaitre, H., Grigis, A., Fischer, C., Dehaene-Lambertz, G., Mangin, J.-F., and Frouin, V. (2019). eQTL of KCNK2 regionally influences the brain sulcal widening: evidence from 15,597 UK Biobank participants with neuroimaging data. Brain Struct. Funct. 224: 847–857.

Lolicato, M., Arrigoni, C., Mori, T., Sekioka, Y., Bryant, C., Clark, K.A., and Minor, D.L. (2017). K2P2.1 (TREK-1)–activator complexes reveal a cryptic selectivity filter binding site. Nature 547: 364–368.

Lolicato, M., Natale, A.M., Abderemane-Ali, F., Crottès, D., Capponi, S., Duman, R., Wagner, A., Rosenberg, J.M., Grabe, M., and Minor, D.L. (2020). K2P channel C-type gating involves asymmetric selectivity filter order-disorder transitions. Sci. Adv. 6: eabc9174.

MacKenzie, G., Franks, N.P., and Brickley, S.G. (2015). Two-pore domain potassium channels enable action potential generation in the absence of voltage-gated potassium channels. Pflüger's Arch 467: 989–999.

Mazella, J., Pétrault, O., Lucas, G., Deval, E., Béraud-Dufour, S., Gandin, C., El-Yacoubi, M., Widmann, C., Guyon, A., Chevet, E., et al. (2010). Spadin, a sortilin-derived peptide, targeting rodent TREK-1 channels: a new concept in the antidepressant drug design. PLoS Biol. 8: e1000355.

Meuth, S.G., Budde, T., Kanyshkova, T., Broicher, T., Munsch, T., and Pape, H.-C. (2003). Contribution of TWIK-related acid-sensitive K^+ channel 1 (TASK1) and TASK3 channels to the control of activity modes in thalamocortical neurons. J. Neurosci. 23: 6460–6469.

Millar, J.A., Barratt, L., Southan, A.P., Page, K.M., Fyffe, R.E.W., Robertson, B., and Mathie, A. (2000). A functional role for the two-pore domain potassium channel TASK-1 in cerebellar granule neurons. Proc. Natl. Acad. Sci. USA 97: 3614–3618.

Moha ou Maati, H., Peyronnet, R., Devader, C., Veyssiere, J., Labbal, F., Gandin, C., Mazella, J., Heurteaux, C., and Borsotto, M. (2011). A human TREK-1/HEK cell line: a highly efficient screening tool for drug development in neurological diseases. PLoS One 6: e25602.

Perlis, R.H., Moorjani, P., Fagerness, J., Purcell, S., Trivedi, M.H., Fava, M., Rush, A.J., and Smoller, J.W. (2008). Pharmacogenetic analysis of genes implicated in rodent models of antidepressant response: association of TREK1 and treatment resistance in the STAR (*) D study. Neuropsychopharmacology 33: 2810–2819.

Pope, L., Arrigoni, C., Lou, H., Bryant, C., Gallardo-Godoy, A., Renslo, A.R., and Minor, D.L. (2018). Protein and chemical determinants of BL-1249 action and selectivity for K2P channels. ACS Chem. Neurosci. 9: 3153–3165.

Pope, L. and Minor, D.L. (2021). The polysite pharmacology of TREK K2P channels. Adv. Exp. Med. Biol. 1349: 51–65.

Ruck, T., Bock, S., Pfeuffer, S., Schroeter, C.B., Cengiz, D., Marciniak, P., Lindner, M., Herrmann, A., Liebmann, M., Kovac, S., et al. (2022). K2P18.1 translates T cell receptor signals into thymic regulatory T cell development. Cell Res. 32: 72–88.

Schewe, M., Nematian-Ardestani, E., Sun, H., Musinszki, M., Cordeiro, S., Bucci, G., de Groot, B.L., Tucker, S.J., Rapedius, M., and Baukrowitz, T. (2016). A non-canonical voltage-sensing mechanism controls gating in K2P K^+ channels. Cell 164: 937–949.

Schewe, M., Sun, H., Mert, Ü., Mackenzie, A., Pike, A.C.W., Schulz, F., Constantin, C., Vowinkel, K.S., Conrad, L.J., Kiper, A.K., et al. (2019). A pharmacological master key mechanism that unlocks the selectivity filter gate in K^+ channels. Science 363: 875–880.

Tertyshnikova, S., Knox, R.J., Plym, M.J., Thalody, G., Griffin, C., Neelands, T., Harden, D.G., Signor, L., Weaver, D., Myers, R.A, et al. (2005). BL-1249 [(5,6,7,8-Tetrahydro-napthalen-1-yl)-[2-(1H-tetrazol-5-yl)-phenyl]-amine]: a putative potassium channel opener with bladder-relaxant properties. J. Pharmacol. Exp. Therapeut. 313: 250–259.

Weaver, C.D., Harden, D., Dworetzky, S.I., Robertson, B., and Knox, R.J. (2004). A thallium-sensitive, fluorescence-based assay for detecting and characterizing potassium channel modulators in mammalian cells. J. Biomol. Screen 9: 671–677.

Wright, P.D., McCoull, D., Walsh, Y., Large, J.M., Hadrys, B.W., Gaurilcikaite, E., Byrom, L., Veale, E.L., Jerman, J., and Mathie, A. (2019). Pranlukast is a novel small molecule activator of the two-pore domain potassium channel TREK2. Biochem. Biophys. Res. Commun. 520: 35–40.

Zhang, J.-H., Chung, T.D.Y., and Oldenburg, K.R. (1999). A simple statistical parameter for use in evaluation and validation of high throughput screening assays. SLAS Discov 4: 67–73.

Zheng, X., Yang, J., Zhu, Z., Fang, Y., Tian, Y., Xie, M., Wang, W., and Liu, Y. (2022). The two-pore domain potassium channel TREK-1 promotes blood-brain barrier breakdown and exacerbates neuronal death after focal cerebral ischemia in mice. Mol. Neurobiol. 59: 2305–2327.

Zheng, Y., Zhu, X., Zhou, P., Lan, X., Xu, H., Li, M., and Gao, Z. (2012). Hexachlorophene is a potent KCNQ1/KCNE1 potassium channel activator which rescues LQTs mutants. PLoS One 7: e51820.

Zobeiri, M., Chaudhary, R., Datunashvili, M., Heuermann, R.J., Lüttjohann, A., Narayanan, V., Balfanz, S., Meuth, P., Chetkovich, D.M., Pape, H.-C., et al. (2018). Modulation of thalamocortical oscillations by TRIP8b, an auxiliary subunit for HCN channels. Brain Struct. Funct. 223: 1537–1564.

Zyrianova, T., Lopez, B., Olcese, R., Belperio, J., Waters, C.M., Wong, L., Nguyen, V., Talapaneni, S., and Schwingshackl, A. (2020). K2P2.1 (TREK-1) potassium channel activation protects against hyperoxia-induced lung injury. Sci. Rep. 10: 22011.

Supplementary Material: This article contains supplementary material (https://doi.org/10.1515/hsz-2022-0266).